Desalination 527 (2022) 115569

Contents lists available at ScienceDirect

Desalination

journal homepage: www.elsevier.com/locate/desal

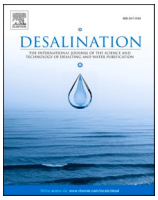

Lithium and magnesium separation from brines by hybrid capacitive deionization

Anna Siekierka

Wroclaw University of Science and Technology, Department of Processing Engineering and Technology of Polymer and Carbon Materials, Wyb. St. Wyspiańskiego 27, 50-370 Wrocław, Poland

HIGHLIGHTS

- Lithium and magnesium separation by HCDI process
- Thermodynamical factors as an explanation of separation Li^+ and Mg^{2+}
- HCDI with LMTO material adsorbed lithium ions with $\beta_{Li/Mg}$ at 2.14 for geothermal brine.

ARTICLE INFO

Keywords:
Separation
Lithium and magnesium brine
Thermodynamics factors
Selectivity
Hybrid capacitive deionization

ABSTRACT

Presented work deals with the problem of separating lithium and magnesium from brines. A similar size of ionic radius characterizes the Li^+ and Mg^{2+}; hence, separating these elements could be problematic. The hybrid capacitive deionization (HCDI) with lithium-manganese-titanium oxides was employed as a potential process for separating lithium and magnesium ions from aqueous solutions. During the investigation, the thermodynamics factors were determined. The enthalpy of activation, the entropy of activation and the Gibbs energy of activation for accumulation Li^+ and Mg^{2+} by Eyring-Polanyi and energy activation by Arrhenius equations were calculated for explanation the separation phenomenon. Next, the HCDI for binary and multicomponent solutions were conducted. The critical role in achieving high $\beta_{Li/Mg}$ plays the activity coefficient of the initial feed, and the value of a voltage applied in constant voltage electric mode. With the increasing value of brines' activity coefficient, the separation factor $\beta_{Li/Mg}$ lift when the concentration of lithium ions decreases. HCDI with LMTO material adsorbed lithium ions with $\beta_{Li/Mg}$ at 2.14 and released Li^+ with over 70% efficiency. The proposed HCDI process employed LMTO sorptive material could be considered a potential method for separating lithium and magnesium from lithium sources.

1. Introduction

Lithium, the third element of the periodic table, has found a wide application in various industrial fields, like medicine or aerospace engineering [1]. However, the demand for lithium has expanded significantly for developing electronic devices, electric vehicles, and portable energy storage, like batteries and capacitors [2]. Lithium can be extracted from land reserves and aqueous resources like brine and salt-lakes, containing almost 25Mt of lithium (62% of total worldwide lithium reserves) [1,3–5]. However, lithium in an aqueous solution exists in the minority with an average concentration at 0.17 ppm for seawater, 0.1–0.2 mg/dm^3 for groundwater, and ~15 mg/dm^3 for geothermal water enriched Li^+ ions [6]. Moreover, one of the biggest challenges to extraction lithium with a high purity level is the high concentration of multiple coexisting ions [7]. Of particular significance is magnesium: the high ratio Mg/Li negative influence of recovery lithium with high purity. Between Mg^{2+} and Li^+ can be distinguished by many similarities due to their diagonal relationship from the periodic table. Lithium and magnesium are often the prototypical isodiagonal pair [8]. They have a similar ionic potential known as a charge to radius ratio (1: 0.59 = 1.7 for Li^+ vs 2: 0.57 = 3.5 for Mg^{2+}) [9,10], high degree of covalency salts, they create a similar organometallic compound [8], and they have a similar ionic radius (for Li^+ radius is around 0.069 nm, for Mg^{2+} is around 0.072 nm) [11]. These figures explain the fact, why Li^+ and Mg^{2+} cations are more strongly hydrated in aqueous solution than heavier congeners (1: 1.02 = 0.98 for Na^+ and 2: 0.99 = 2.0 for

E-mail address: anna.siekierka@pwr.edu.pl.

https://doi.org/10.1016/j.desal.2022.115569
Received 25 October 2021; Received in revised form 6 January 2022; Accepted 13 January 2022
Available online 20 January 2022

Ca^{2+}) [12,13]. The above similarities provide an issue in separating lithium and magnesium, especially with higher ration Li/Mg. Most lithium-containing salt lakes have an Mg/Li ratio between 1 and 10, but in some cases, this factor could riches a level of around 1000 (deposits in Qinghai-Tibet plateau [14]). The detailed representatives for lithium-contain aqueous deposits are summarized in Table 1. Based on the data, the lithium concentration does not exceed 0.3% *w*/w, classified as ultra-diluted. Moreover, the ratio Mg/Li is maintained below 10. The average Mg/Li ratio in brines is eight, while the lithium concentration is ranged from 10 to 1000 mg/dm^3 [2]. Therefore, developing a high-efficiency and low-cost method for treating high Mg/Li brine with highly selectively properties is necessary.

Nowadays, a few techniques that deal with the separation of Mg/Li from brines could be distinguished [15]. There are extraction, including solvent extraction [16], ionic liquid extraction [17–19] and neutral extraction [20,21], deep eutectic solvent extraction [22], adsorption methods based on application selective sorbents like aluminium-based spinel's [23–25], manganese-based spinel's [26,27,28], titanium-based spinel's [29–32], as well as membrane methods including nano-filtration [33–37], electrodialysis [38–40], electrodialysis with bipolar membranes [41], membrane capacitive deionization [42,43] and electrochemical methods [44–46] dedicated for lithium capturing. Most of these methods applied additional reagents and required the exceed time and conditions to predict lithium removal.

The hybrid capacitive deionization process with fast adsorption and desorption operations is proposed to deal with these problems. The hybrid capacitive deionization (HCDI) method is recognised as a selective ion capture process. The principle stack of HCDI comprises two parallel electrodes divided by a polymeric separator, allowing continuous flowing feed and permeate solutions [53–55]. Among electrodes, the cathode and anode can be distinguished. The cathode is built from selective sorbent based on spinel-type materials, while the anode is constructed from a connection anion-exchange membrane and electrode made with activated carbon [51,56–59]. The research delivers information about the selective sorption of lithium from geothermal brines. [60]. Thanks to manipulating electrical modes, the lithium could be released from multicomponent solution with over 70% efficiency with reduction Na:K:Li ratio from 227:1:1.1 to 2.9:0:1 by one processing cycle [61]. Hence, the idea related to further investigations of the separation of Li and Mg from aqueous solutions is reasonable.

This paper presents the research under the separation of lithium and magnesium from mono, binary and multicomponent systems. The primary purpose was to understand the separation mechanism and deliver knowledge about separation behaviour and its limit. The research under the influence of other ions on selective separation mixtures of Li/Mg was investigated to achieve this. The next goal was to compare the selective sorbents under separation factor research and the performances dedicated to CDI technologies like electrical modes, power efficiency, energetical efficiency, and salt adsorption capacities.

Table 1
Properties of known depositions in the world [5,47–52]. *n.s.* – not specify.

Deposit	Country	Li, % *w*/w	Mg, % w/w	Mg/Li	Ref.
West Taijnar Salt lake	China	0.2	12.6	60	[47,48]
Atacama Salar Brine	Chile	0.15	0.96	6.4	[5,52]
Uyuni Salar Brine	Bolivia	0.045	0.9	20	[5,52]
Great Salt Lake	USA	0.04	10	250	[5,52]
DXC	China	0.033	0.008	0.25	[5,52]
Zabuye	China	0.097	0.00097	0.01	[5,52]
Hombre Muerto	Argentina	0.062	0.085	1.37	[5,52]
Olaroz	Argentina	0.07	0.196	2.8	[5,52]
Maricunga	Chile	0.092	0.736	8	[5,52]
Dead sea	Izrael	0.002	3.4	1700	[5,52]
Fox creek	Canada	0.01	0.1	10	[5,52]
Smackover	USA	0.037	0.074	20	[5,52]
Silver Peak	USA	0.03	0.04	1.33	[5,52]
Cinovec	Czech Republic	0.2	n.s	n.s.	[50]
Seawater	n.s.	0.00017	1.19	7000	[49]
Geothermal water	n.s.	0.015	n.s.	n.s.	[51]

2. Materials and methods

2.1. Materials

For HCDI tests, the following materials were used: lithium chloride, >99%, Sigma-Aldrich, magnesium chloride hexahydrate, >99% Stanlab, Poland, potassium chloride, 99%, Avantor Performance Materials, sodium bicarbonate, 99%, Avantor Performance, Materials, Poland, calcium carbonate, 99%, Merck, cyclohexanone (CH), >99%, Sigma-Aldrich. In addition, deionized water (DI) was delivered from RO Water Purification Systems Millipore (15MΩ/cm^2), PVC powder (Ongrovil S-5167) supplied by BorsodChem (molecular weight of 52,000 g/mol).

2.2. Materials characterisation

The LMTO before and after Li/Mg separation was analysed by X-ray diffraction (XRD) techniques using a Philips X-Pert PW 3040/60 diffractometer (Kα = 1.5418 Å) and a Cu lamp (30 mA and 40 kV). All of the measurements were determined in the range of 2θ angles between 5° to 120° at 25 °C with a rate 3 °C/min in 0.02° steps. The porous structure of sorptive materials was analysed by using the 77 K N_2 sorption method using an Autosorb IQ gas sorption analyser. The specific surface area was calculated according to the Brunauer-Emmett-Teller isotherm procedure. The total pore volume was recognised from adsorbed nitrogen at p/p0 = 0.95. The ^{7}Li NMR was studied using a Bruker Avance III 400WB spectrometer with a magic angle spinning probe (MAS). The sample was situated in a zirconium oxide rotor (4 nm) and centrifuged at 10 to 14 kHz. A single pulse excitation sequence followed by free induction decay was used for spectra recording. The excitation pulse duration and the delay time were 0.5 μs and 5 s for ^{7}Li NMR. The one spectra were estimated as a result of averaging 64 scans. Also, the samples were stabilized at room temperature. The obtained results are stored at the Centre of Magnetic Resonance of the University of St. Petersburg, Russia, under ID 7094 (no. 80356, 80424, 80475, 80579, and 80665). The surface energy characterisation was analysed by contact angle measurements using a PG-X goniometer (Fibro Systems). During measurement, the three liquids probes like demineralized water (polar), diiodomethane (nonpolar) and formamide (half-polar and half-nonpolar) were used.

The contact angle values were obtained by averaging 10 repetitions. The harmonic averaging protocol was applied for investigated the surface free energy (γ) and its basic (γ_b) and acidic (γ_a) components.

The AEM was characterized by determining the ion exchange capacity (IEC), water uptake, content of nitrogen, contact angle of water. The ICE was estimated by the acid-base titration method. The membrane was kept in 0.1 M NaOH solution for 24 h, and at that time, a 10 mL of the solution was taken for titration by 0.1 M HCl. The IEC was calculated as a ratio of differences between NaOH and HCl volume (with known concentration) sorbed by a membrane to the mass of a dry sample of the membrane (100 mg). The water uptake was determined as a ratio of a soaked membrane sample to the mass of the dry membrane. Kjeldahl's method determined nitrogen content (ZN) after mineralization of the sample (about 100 mg) in concentrated sulphuric acid with copper and potassium sulphates.

2.3. Sorptive material and electrode preparation

The adsorbent Li-TiO_2-MnO_2 (LMTO) with 5% TiO_2 and ratio Li:Mn:Ti at 1:3:0.15 was chosen to build selective cathode while activated carbon (AC) YP-50F received from coconuts delivered by Kuraray Chem

Co., Japan to the made counter electrode. Also, the CWZ-22 activated carbon (Gryfskand, Poland) obtained from wood was used for comparison of the separation factors. The characterizations of ACs are presented in Table 2. The preparation procedure and exceed properties can be found in previous papers [51,59,62]. All of the electrodes were prepared by mixing 90 wt% of sorptive materials with ten wt% of poly (vinyl chloride) mixture (3.5 wt% solution PVC in cyclohexanone), according to [59]. Before mixing, the powder materials were dried at 80 °C overnight. Then, the cooled powders were added to a PVC/CH solution and stirred for 30 min at 40 °C in an ultrasonic reactor (CNC-Ultrasonic, PS 30A), separately for LMTO and AC. Finally, the slurries were cast on the current graphite collector, and electrodes with 80 μm of thickness by casting knife were formed. The solvent was firstly removed by evaporation at 60 °C for 24 h and later in a vacuum dryer. Next, electrodes were immersed, kept in demineralized water, and rinsed before application at the HCDI system (Fig. 1).

In addition to obtaining the final anode in the HCDI system, the anion exchange membrane (AEM) is added on the top of the formed AC electrode. The modified poly(vinyl chloride) by ethylene diamine (PVC-EDA) by five days at room temperature was chosen to represent AEM. The film of PVC was immersed in pure EDA to predict the reaction between chloride atom and amine [63]. After modification, AEM was rinsed with methanol, ethanol, ethanol/water (ratio 50:50) and kept in demineralized water. As a result, the membranes change the colour from transparent film to deep brown. Before use, AEM was hydrolyzed by immersion in a mixture of ethanol in demineralized water (50 wt%). The properties of used AEM can be found in Table 2, while the detailed preparation and exceed characterisation procedure is delivered in [63,64].

2.4. HCDI configuration

The FT-ED-100-4 (FumaTech) electrodialyzer was employed as an HCDI cell assembly to study lithium and magnesium separation. The HCDI stack comprised two parallel electrodes divided by a polymeric spacer channel with 200 μm of thickness. The LMTO material was used for cathode building while the AC, YP-50F, was applied as an active anode material. An anion exchange membrane, PVC-EDA, also covered the anode electrode. The CWZ-22 AC was applied for cathode building; however, it was used to compare separation performances to LMTO.

The electrodialyzer was biased by Multi-Range programmable DC Power Supply BK Precision 9201 and controlled by DC Electronic Load BK Precision 8601. The tests were conducted under constant voltage (CV) electrical mode during single and binary component solutions. For a multicomponent solution, the combination of electrical modes was chosen. In addition, the CX-601 multimeter was applied to monitor conductivity, pH and temperature of feed and permeate during HCDI tests. The conductivity measurement of solutions was performed to control any differences in feed and permeates. The pH was checked to control any water splitting and side reactions. Finally, the temperature was checked to observe the sorption effect, usually exothermic.

2.5. HCDI calculations

Fundamental factors for the capacitive deionization process, like salt adsorption capacity (SAC), salt desorption capacity (SDC) and average salt adsorption rate (ASAR) and average salt desorption rate (ASDR), were calculated. The SAC determines the adsorbed salt (represented by a single ion) per gram of applied active material (90% of total electrode weight), while SDC represents the desorbed salt. When the amount of adsorbed/desorbed salt was normalized to the processing time, it calculated the average salt adsorption/desorption rate (ASAR/ASDR), a valuable metrics for process description. The SAC, ASAR and SDC, ASDR indicates the general adsorption/desorption capacity and rate delivered from initial and final concentrations of ions or online according to the time step. Furthermore, during calculation related to energy consumption and charge/current efficiency, the results obtained by performing the measurements without an external electrical field reduced the adsorption. This case shows how the electrical potential/current influences charge/current efficiency and adsorption/desorption behaviours.

The simple RC circuit with measurements of current change was applied to analyse the energy consumption and calculate the system capacity. First, the energy consumption (EC) was computed from numerical integration of the current versus time relationship and voltage. Then, the following metrics were energy normalized adsorption/desorption of salt (ENAS and ENDS) in gram units per Joule of energy. The next factor describing HCDI was electrical work in Wh per gram of adsorbed/desorbed salt, and it was defined as a ratio of charge flow by the system during the adsorption/desorption step an electrical potential between electrodes the mass of adsorbed/desorbed salt.

2.6. Solutions determinations

During tests, the single, binary and multicomponent solutions were investigated. To determine the concentration of particular elements, the following methods were chosen. Chloride concentrations. Chloride was measured according to the Mohr method based on calibration curves. Magnesium and calcium concentrations. The Mg^{2+} and Ca^{2+} were measured by colourimetric titration by EDTA in the presence of two indicators: Eriochrome T (sum of both cations) and ammonium purpurate (mass of calcium). Simple mass balances determined the mass of magnesium. Potassium, lithium and sodium were analysed at the accredited laboratory (PCA-AB 1050 and PCA-AB 176) by Inductively Coupled Plasma Optical Emission Spectrometer, ICP-OES (Optima 7300DV). The details about samples' preparation and measurements are presented elsewhere [57]. Conductivity, pH and temperature. The conductivity method determined the salt concentrations in applied monocomponent solutions during HCDI tests. For investigation on authentic geothermal sources, the water from Warzelnia intake was selected. The general conductivity of the solution was 33.5 mS/cm. The characteristics of applied brine are shown in Table 3.

Table 2
Characteristic of used electrode materials and anion-exchange membrane [51,64,65].

Type of material	Specific surface area [m^2g^{-1}]	Pore volume [cm^3g^{-1}]	Pore diameter [nm]
YP-50F	~1600	0.757	1.65
CWZ-22	~800	0.51	0.3–0.7

Type of material	Dominated exchange groups	Ion exchange capacity [$mmolg^{-1}$]	Content of nitrogen [$mmolg^{-1}$]	Water uptake [gg^{-1}]	The contact angle for water [°]	The polarity of surface [%]
PVC-EDA	Amines ($-NH_2$)	1.4	2.3	1.0	36	33.4

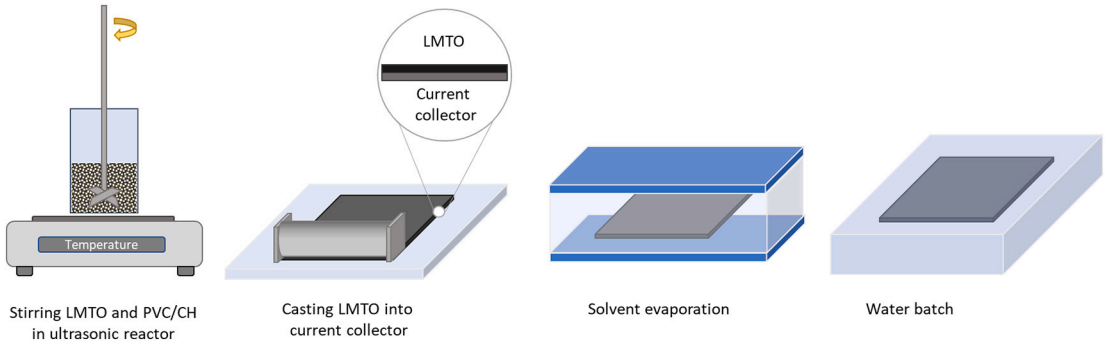

Fig. 1. Scheme of procedure of electrode LMTO and AC preparation.

Table 3
Chemical characterisation for geothermal water from Warzelnia intake.

Li^+ (mg/dm^3)	Mineralization (mg/dm^3)	TDS (mg/dm^3)	pH	Hardness (mg_{CaCO3}/dm^3)	B (mg/dm^3)	Si (mg/dm^3)
12.6	20,800	20,100	7.87	301	110	7.8

Na^+ (mg/dm^3)	K^+ (mg/dm^3)	Ca^{2+} (mg/dm^3)	Mg^{2+} (mg/dm^3)	Sr^{2+} (mg/dm^3)	Cl^- (mg/dm^3)	HCO_3^- (mg/dm^3)
7363	80	57.6	38.2	17.9	11,252	1419

3. Results and discussion

3.1. HCDI Li^+ and Mg^{2+} ions transportation and energetical factors

The HCDI technology was applied to investigate the differences in Li^+ and Mg^{2+} transportation and separation properties. The primary HCDI cell was composed of spinel-type lithium-manganese-titanium oxide with 5% *w*/w as active material in the cathode material (90% *w*/w). At the same time, composite anode built with activated carbon electrode coated by an anion-exchange membrane, PVC-EDA, were selected to investigate the initial conditions for lithium and magnesium ions separation from mono, binary and multicomponent solutions. The initial tests were performed with monosolutions of lithium and magnesium cations, dedicated to selecting the best voltage value in constant voltage electrical mode during charging.

The active cathode (LMTO) material accumulated lithium ions within its crystal phases and predicted the exchange reaction between lithium and hydrogen [60]. Fig. 2A and B shows the modified Ragone plot for lithium and magnesium ions, respectively, during various voltage applications. At U = 0 V, ions are accumulated on electrodes according to first and second Fick's law, while with application electrical mode, the following driving forces as an external electrical field have appeared. The improved accumulation of lithium ions in LMTO active material is seen with the applied external electric field. With U = 2 V, the SAC riches 14 mg/g of Li^+, while for U = 0 V, the SAC value is 3 mg/g of Li^+. Hence, the external electrical field increases the effect of sorption lithium ions in cathodic material over four times. This behaviour is not observed in the sorption of Mg^{2+} (Fig. 2B). The SAC of Mg^{2+} ions at U = 0 V reached 3 mg/g, whereas, at U = 2 V, this value has 7.7 mg/g. As a result, the external electrical field increases the SAC of Mg^{2+} ions over two and half times.

Overall, the SAC has two times the higher value for Li^+ than for Mg^{2+} ions. The same situation is observed at the ASAR parameter. The ASAR parameter described sorption rate. The most vital difference in comparing the ASAR values is the shape of the received curve ASAR vs SAC, which indicates the kinetics of sorption or desorption operations. Moreover, the modified Ragone plot (mRP) as a crucial CDI parameter was discovered by Kim and Yoon [66]. They provided the range of ideal performances of CDI, where the capacity of sorption is predicted at an optimal rate. The grey regions in Fig. 2A and B show the ideal conditions for CDI charging operation. From comparing the Li^+ and Mg^{2+} mRP, the ideal conditions of CDI reached only the lithium sorption with an applied external electric field. Based on these results, the optimal voltage at constant voltage (CV) electrical mode for lithium sorption ranges from 1 V to 2 V.

The next factor described in the HCDI process is the Ragone plot (RP). The RP is used to determine the specific energy (Wh/g) plotted versus specific power (W/g) for different sources working under the external electric field. The Li^+ and Mg^{2+} energetical requirements results are presented in Fig. 2C and D, respectively. The specific energy and power results are calculated over 1 g of particular cations (separately for Li^+ and Mg^{2+}). With increasing the external voltage, the consumption of energy is raised. The tendency of required energy and power depends on applied voltage; in both cases, systems reached similar values of specific energy; however, the specific power exposed significant differences at U = 1 V.

The following crucial parameter is related to differences in accumulation and transportation of lithium and magnesium ions depending on the applied voltage. The results are summarized in Fig. 2E (for lithium ions) and 2F (for magnesium ions). Significant differences are seen between applied and not applied external electric fields for lithium ions transportation. Based on the theory of Nernst-Planck-Poisson of mass transportation within the electrical field, the three elementary components of ions accumulation can be distinguished [53]. The component is related to concentration gradient where the central role plays the first and second Fick's laws, the component of electrostatic potential responsible for migration and convection component connected with the velocity of moving species. This theory of mass accumulation with and without external field could be working for only membrane processes; here, it cannot be neglected type of used material for accumulation ions. In both cations and anions, the accumulation mechanism depends on the electrode materials; hence, the accumulation of ions within LMTO cathode material will be decided about selective capturing lithium or magnesium. Furthermore, LMTO is strongly dedicated to lithium accumulation based on exchange reaction within their crystalline structure between $Li^+ \leftarrow\rightarrow H^+$, reactions with manganese and accumulation in EDLs (electric double layers) [6,60]. This behaviour is observed in Fig. 2E and F. The accumulation of ions in both cases was around 10% within the applied external electric field. The phenomena could explain the above fact associated with Mg^{2+} sorption in EDL only; hence, the specific surface area is prominent. For Li^+ cations, the sorption is related to a specific reaction in an external field, explained in [60].

The desorption phenomenon during HCDI was controlled. The data is presented in Fig. 2G and H for Li and Mg desorption. In both cases, the desorption riched almost ~90%. Only for lithium separation, the modified Ragone plots got the ideal performances of the amount of

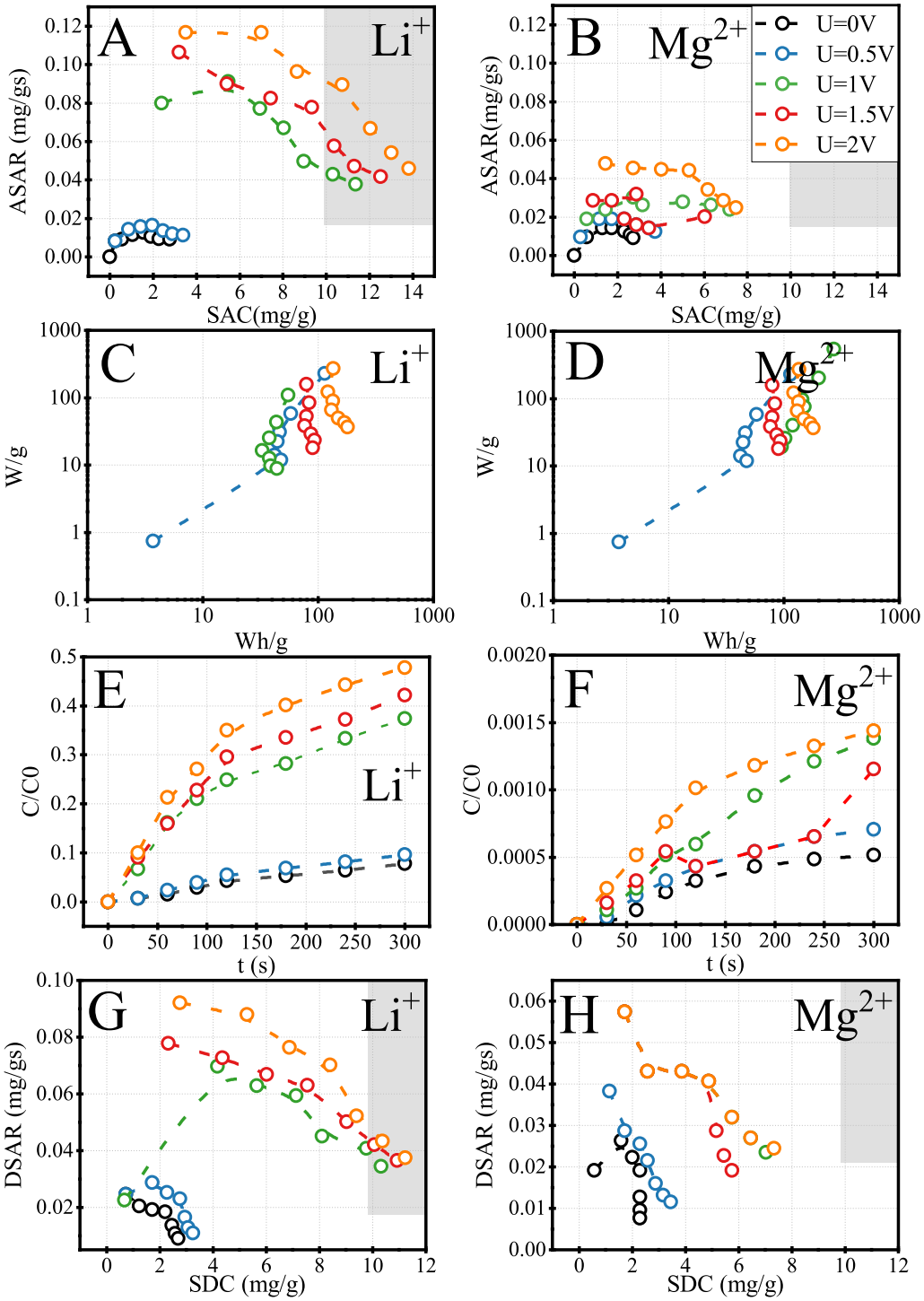

Fig. 2. HCDI factors over various voltage as modified Ragone plots during charging for Li^+ (A), Mg^{2+} (B), Ragone plot for Li^+ (C) and Mg^{2+} (D), rates of sorption over time for Li^+ (E) and Mg^{2+} (F) modified Ragone plots during discharging for Li^+ (G) and Mg^{2+} (H). Process conditions: concentration of Li^+ and Mg^{2+} was 15 mmol/dm^3, the flow rate was six dm^3/h, charging and discharging were 5 min equally, V_{feed} = 0.1 dm^3.

desorbed Li and rate of achieved this desorption (grey region). The rate of desorption in Li and Mg is promising and ensures that the HCDI can be effectively used for the sorption and desorption of ions.

3.2. *Thermodynamics of lithium and magnesium transportation via HCDI*

Thermodynamics factors show the differences in Li and Mg transportation through HCDI. Previously, we detected that the mechanism of accumulation of lithium ions in LMTO material is related to the ion-exchange reaction between $Li^+ \leftarrow\rightarrow H^+$ and disproportion reaction of manganese atoms from LMTO [51,60]. Hence, the energy activation for interaction cations with hydrogen and manganese sites could give insight into the transport mechanism through selective spinel-type material. To calculate the energy activation Eq. (2) is applied:

$$k = Ae^{\frac{-Ea}{RT}} \tag{2}$$

The Eyring-Polanyi equation was applied to calculate the Gibbs energy and state functions of complexed cations-hydrogen and manganese

sites. The general form of the Eyring-Polanyi equation is shown below:

$$k = \frac{\kappa k_B T}{h} e^{\frac{-\Delta G_i^{\ddagger}}{RT}} \quad (3)$$

where ΔG‡ is the Gibbs energy of activation, k_B is Boltzmann constant, h is Planck's constant and κ is the transmission coefficient.

The κ could be assumed to be equal to one, reflecting what fraction of the flux proceeds without recrossing the transition state. Hence, the transmission coefficient equal to one means that the fundamental no-recrossing assumption of transition state theory holds perfectly. So now, the Eyring-Polanyi equation can be rewritten as:

$$k = \frac{k_B T}{h} e^{\frac{\Delta S_i^{\ddagger}}{R}} e^{\frac{-\Delta H_i^{\ddagger}}{RT}} \quad (4)$$

Furthermore, its linear form looks as follows:

$$ln\frac{k}{T} = \frac{-\Delta H^{\ddagger}}{R} \bullet \frac{1}{T} + \ln\frac{k_B}{h} + \frac{\Delta S^{\ddagger}}{R} \quad (5)$$

where ΔH‡ is the enthalpy of activation, ΔS‡ is the entropy of activation, and T is the temperature in K.

The results from the linearization of Eqs. (2) and (5) are summarized in Table 4.

The initial study indicates the determination of the activation energy of lithium and magnesium cations. The Li^+ and Mg^{2+} cations concentrations were measured at different temperatures in 24.4 °C–33.6 °C. The transport phenomena selected cations in different temperatures is presented in Fig. 3A the relationship between $\ln(C/C_0)$ and t exhibit significant differences in Li^+ and Mg^{2+} transportation. The k values increased with increased temperature; consequently, the total sorption was higher. For Mg^{2+} cations, their total sorption increased from 3.3% to 5.0% by temperature rise on 9.2 points. The k values rise from $2.9 \bullet 10^{-8}$ to $3.8 \bullet 10^{-8}$. For Li^+ cations, their total sorption elevated up from 20% to 25% by temperature rise on 9.2 points. The k value in the case of Li^+ accumulation for 24.4, 28.6, 33.6 reached $1.5 \bullet 10^{-7}$, $1.9 \bullet 10^{-7}$, $1.95 \bullet 10^{-7}$, respectively. The system with LMTO materials allows extracting five times more lithium than magnesium cations. The date is plotted as ln*k* versus *1/T* to obtain the activation energy from the slope of the curves (Fig. 3B). The calculated activation energies for complex formation Li^+-LMTO and Mg^{2+}-LMTO are listed in Table 4. According to them, the lithium cation exhibits a lower value of E_a than the complex Mg^{2+}-LMTO over 15%. Generally, the lower activation energy of complexation results in faster transportation of particular cations. Hence, the LMTO system enhanced the transport and complexation of lithium cations.

The Eyring-Polanyi equation is helpful for investigation ΔH‡, ΔS‡ and ΔG‡. The molecularity of the rate-determining step, like the reactants affinity, could be recognised by ΔS‡ according to differences in values. The positive value is related to the rising transition state and demonstrates a complex creation's dissociation mechanism. In contrast, the negative values could associate with the mechanism of two reactants forming within the activated complex. Hence, together with the entropy of activation, the Gibbs energy of activation could be considered self-sufficiency indicators. For capturing Li^+ and Mg^{2+} the requirements for self-sufficiency were met for $\Delta S^{\ddagger} > 0$ and $\Delta G^{\ddagger} < 0$. It meant that the LMTO material could sorb the Li^+ and Mg^{2+} cations.

Table 4
Enthalpy of activation, the entropy of activation and Gibbs energy of activation for accumulation Li^+ and Mg^{2+} by Eyring-Polanyi equation and energy activation by Arrhenius equation.

Type of cation transportation	ΔH‡ [J/mol]	ΔS‡ [J/K·mole]	ΔG‡ [J/mol]	E_a [cal/mol]
Li^+	221.5	1.17	−96.5	297.9
Mg^{2+}	277.9	1.15	−34.8	354.5

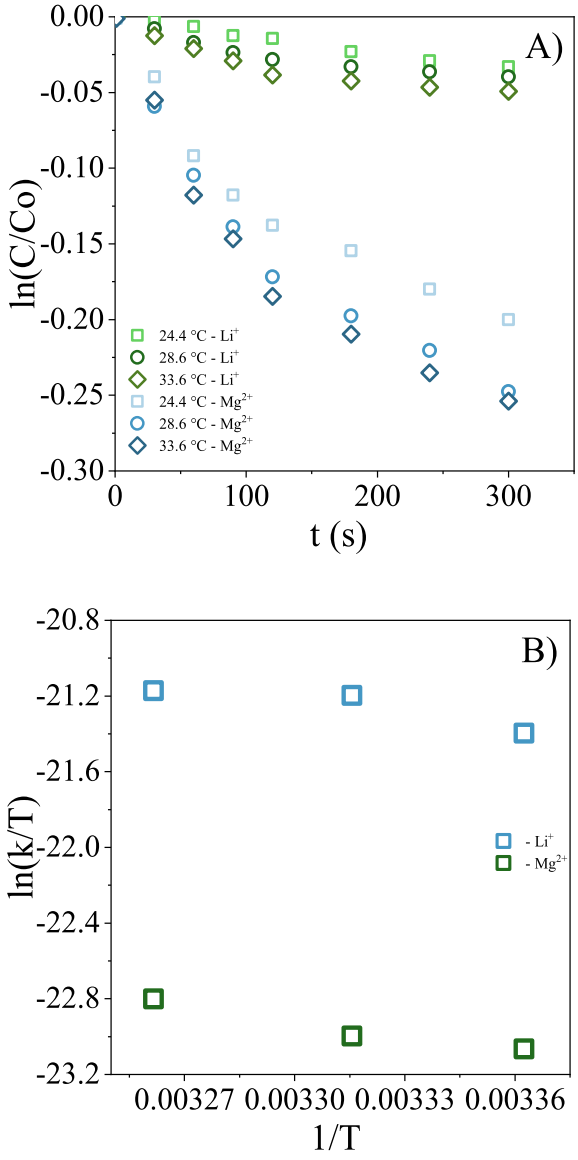

Fig. 3. Linearization of Li^+ and Mg^{2+} transportation (A), and plot of ln(k/T) vs 1/T according to Eyring-Polanyi equation (B).

The change of Gibbs energy of activation can equal the system's work. Hence, the value of ΔG‡ should equal electrical work that can be collected. This fact is essential for applying LMTO material in the electrical system and can be helpful for energy storage.

3.3. Selective separation binary solution of Li^+/Mg^{2+}

Evaluating properties dedicated to lithium removal from aqueous solution requires comparing selective factors by applying two-component solutions.

In the first case, the initial solution's equal molar ratio of Li^+ and Mg^{2+} (1:1) was applied. The salt adsorption capacity, sorption rate, selectivity, and energetical factors were evaluated. The data are presented in Fig. 4. In the beginning, the sorption factors as SAC vs ASAR for Li^+ (Fig. 4A) and Mg^{2+} (Fig. 4B) were studied. In the HCDI system, the binary solution of Li^+ and Mg^{2+} with the molar ratio of 1:1 were employed. In this case, the effect of the external electrical field for selective separation of lithium from a binary mixture of Li and Mg was studied. At the same time, the molar concentration (20.6 mmol/dm^3 in initial solution) of both individuals were measured. In different values of

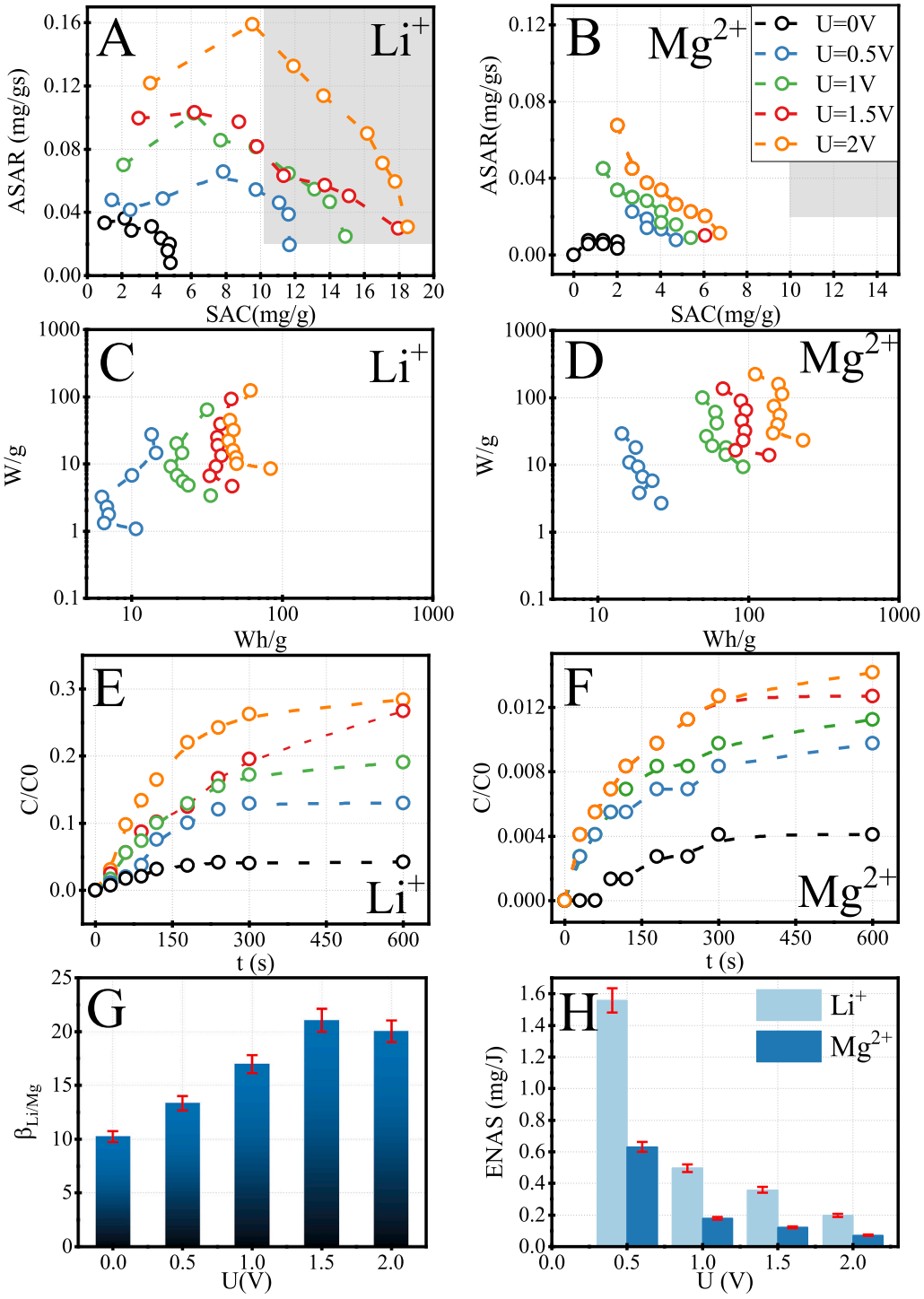

Fig. 4. HCDI factors over various voltage during charging of binary solution of lithium and magnesium. Modified Ragone plot for Li^+ (A), Mg^{2+} (B), Ragone plot for Li^+ (C) and Mg^{2+} (D), rates of sorption over time for Li^+ (E) and Mg^{2+} (F) selectivity of Li^+/Mg^{2+} (G) and ENAS for Li^+ and Mg^{2+} (H). Process conditions: the total concentration of Li^+ and Mg^{2+} was 41.2 mmol/dm^3, the flow rate was six dm^3/h, charging and discharging were 10 min equally, V_{feed} = 0.1 dm^3.

CV mode, the effect of Li/Mg separation was evaluated. The grey region marked at those two graphs indicates the ideal performances dedicated for the CDI system according to [66]. From comparison data in Fig. 4A and B, it could be concluded that the ideal performances of CDI were reached only by lithium ions despite the presence in solution magnesium ions. The SAC for Li^+ was 2–4 times higher in all CV modes, even for the test without an external electrical field (U = 0.0 V). Also, the rate of sorption represented by the ASAR factor had several times higher values. Describes effects are directly connected to data present in Fig. 4E and F, where the sorption in terms of C/C_0 over time for Li^+ and Mg^{2+} were reported. Here, it can be concluded that the sorption of Li^+ reached ~28% per one cycle, while the sorption of Mg^{2+} met ~2% at the same examination. The effect of application rising voltage at CV modes directly influences the growing SAC and C/C_0 in the sorption of both detected individuals. Hence, applying an external electrical field does directly impact total sorption. The external electric field in different CV values has also leveraged energy consumption. The classical Ragone plots for lithium and magnesium ions are presented in Fig. 4C and D.

For lithium the energy consumption from 10.7 Wh/g (74.4 Wh/mol of Li^+) for U = 0.5 V to 84 Wh/g (583 Wh/mol of Li^+) for U = 2.0 V, respectively. For magnesium the energy consumption 26.4 Wh/g (642.3 Wh/mol of Mg^{2+}) for U = 0.5 V to 230.4 Wh/g (5605.8 Wh/mol of Mg^{2+}) for U = 2.0 V. Hence, the energy consumption in the sorption of both ions increases eight times, while SAC of Li^+ rises ~3.8 times and SAC of Mg^{2+} rise about 3.5 times. The main differences over the applied external electric field in CV mode are comparison selectivity factors Li/Mg. The data for the selective factor of Li/Mg are summarized in Fig. 4G. According to the graph, the selective factor increases with the external electric field in changing voltage in CV modes. The selectivity factor Li/Mg promotes a particular element's sorption (electrosorption). By applying external electrical mode, the $\beta_{Li/Mg}$ rises from 10 for U = 0.0 V to over 20 for U = 2.0 V. Hence, the system comprised of LMTO material can be a good candidate for sorbent lithium ions from binary solution without an external electrical field. However, with application CV modes with U = 2.0 V, the $\beta_{Li/Mg}$ reached two times higher value. Considering the separation factor, both phenomena as selective sorptive material and conditions of the HCDI process have a key role in selective separation lithium from binary solution, where the cations have a similar ionic radius. The last parameter describing Li and Mg separation from aqueous solution by HCDI is ENAS; normalized energy exposes how many grams of salt can be sorbed per one Joule of energy. The data is presented in Fig. 4H. The highest ENAS was obtained for lithium sorption in the minimum chosen U = 0.5 V. With increasing the voltage in CV electric modes, the ENAS for lithium ions decreased and achieved

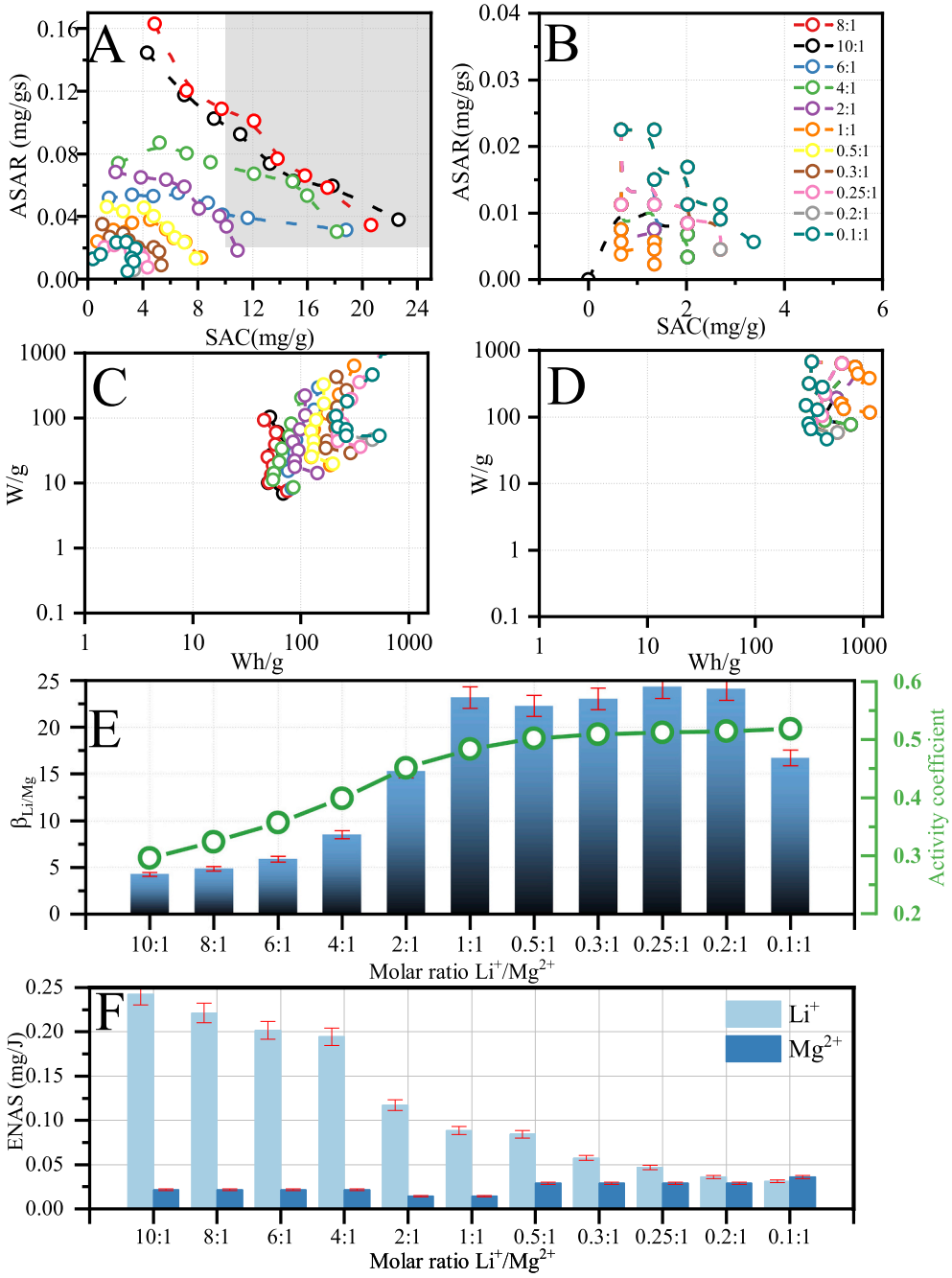

Fig. 5. HCDI factors over the various initial molar ratio of binary solution Li/Mg for charging. Modified Ragone plot for Li^+ (A), Mg^{2+} (B), Ragone plot for Li^+ (C) and Mg^{2+} (D), selectivity of Li^+/Mg^{2+} and activity coefficient of initial binary solution over initial molar ratios of Li/Mg (E) and ENAS for Li^+ and Mg^{2+} (F). Process conditions: the flow rate was six dm^3/h, charging was 10 min equally, V_{feed} = 0.1 dm^3, U = 2.0 V.

0.2 mg/J for U = 2.0 V. The same situation can be observed for magnesium releasing, where with increasing voltage, the ENAS folded down and finally reached 0.07 mg/J. In summary, the normalized energy decreases with higher voltage in CV electrical mode in lithium and magnesium electrosorption.

The next series of evaluation HCDI systems for selective removal of lithium from binary solution assumes the comparison of electrosorption Li and Mg from solutions where their initial molar ratios were variables from 10:1 to 0.1:1 in terms of ratio Li to Mg. In the beginning, the modified Ragone plot exposes SAC vs ASAR for Li^+ and Mg^{2+}. The sorptive factors were compared. The investigated molar ratio Li/Mg were 10:1, 8:1, 6:1, 4:1, 2:1, 1:1, 0.5:1, 0.3:1, 0.25:1, 0.2:1, 0.1:1. The results are presented in Fig. 4A and B. Similar to the previous series, the ideal conditions for the modified Ragone plot were reached only for lithium sorption, according to Fig. 5A and B. The highest sorption of lithium ions was achieved for the solution with Li/Mg at 10:1 and 8:1; moreover, the tendency to accumulate L^{1+} decreased with the increasing contribution of Mg^{2+} in initial solutions. Therefore, the highest SAC and ASAR for Mg^{2+} took place for 0.1:1 M ratio Li/Mg. The inclination of electrosorption for lithium is inversely proportional to magnesium behaviour, considering the initial molar ratio Li/Mg of solutions. For lithium sorption, the SAC decrease from ~23 mg/g to 3.5 mg/g for 10:1 and 0.1:1 M ratio, respectively. Reduce sorption by 6.5 times. In contrast, the SAC of Mg2+ rises from 2 mg/g to 3.2 mg/g, enhancing sorption by 60%. The initial molar ratio of Li/Mg has a crucial impact on lithium sorption due to a decrease of 100 times their concentration; however, the impact on Mg^{2+} seems to be not too strong. The SAC and ASAR increase with marginally little influence of real differences between both studied individuals.

The next factor is related to the classical Ragone plot that exhibited the preferences for energy consumption. Fig. 5C and D shows the Ragone plot obtained during electrosorption of binary solutions. With the increasing content of Mg^{2+} in the initial solution, the energy consumption for Li^+ removal increased linearly from 68.7 Wh/g (477 Wh/mol of Li^+) to 533.4 Wh/g (3704 Wh/mol of Li^+). On the other hand, in the case of Mg^{2+} sorption, the consumption fell from 768 Wh/g (18.7 kWh/mol of Mg^{2+}) to 460.8 Wh/g (11.2 kWh/mol of Mg^{2+}). Despite that, the energy consumption in the case of magnesium sorption decreasing its value is still substantial and cross the energetical barrier for the typical energy consumption for the CDI process [67]. The following key parameter evaluated during research is separation factor $\beta_{Li/Mg}$. The data is presented in Fig. 4E. According to investigations, the separation factor $\beta_{Li/Mg}$ increases with decreasing molar fraction of lithium contribution in the initial solution.

This phenomenon is directly related to the activity coefficient of solutions and their ionic strength values. The ionic strength is expressed as:

$$I = \frac{1}{2}\sum_{i=1}^{n} c_i z_i^2 \tag{6}$$

where c_i is a concentration of ion (both Li and Mg), z_i is a charge sign (for Li^+ it is +1 and for Mg^{2+} is +2) and can affect Li^+ and Mg^{2+} activity coefficient, f_i, according to

$$logf_i = -0.5 z_i^2 \sqrt{I} \tag{7}$$

The above equations show that dilution causes a decrease in ionic strength and increased activity coefficient (f_i). With increasing f_i, the $\beta_{Li/Mg}$ rose and reached over 20 for an initial molar ratio above 1:1. This behaviour is directly influenced by changing the concentration of lithium ions in the initial solution and saving the stable concentration of magnesium ions, which changes the activity coefficient, presented by the green series in Fig. 5E. The next factor is related to the particular accumulation amount of ions per one Joule of energy, ENAS, over the initial molar ratio of Li/Mg. The ENAS has the highest value, 0.25 mg/J, for lithium ions at the highest molar ratio, Li/Mg 10:1, and linearly decreased to below 0.05 mg/J. Hence, the ENAS fell by five times. The oppositive situation took place in sorption of Mg^{2+}, where the ENAS was rising with increasing content of Mg^{2+} in the initial solution., from 0.2 mg/J at Li:Mg = 10:1 to 0.4 mg/J at Li:Mg = 0.1:1. Combining the data from Fig. 5E and F, the separation factor has a proportional relationship with ENAS for Mg^{2+} cations and is inversely proportional with ENAS for Li^+ cations.

In summary, the $\beta_{Li/Mg}$ is related to the activity coefficient of the applied initial solution evaluated for lithium and magnesium separation. Despite the high content of Li^+ at 10:1 M ration solution, the $\beta_{Li/Mg}$ reached ~5. This fact is caused due to the maximum sorption capacity of applied LMTO material (from 0.1 M LiCl by 24 h without external electric field, the SAC_{max} was 28.6 mg/g, where the available theoretical SAC_{theor} was 71 mg/g). Hence, the leak of separation factor is caused by the higher available mass of Li + than the system within 10 min can sorb. However, the most promising information is the negligibly small sorption of Mg^{2+} through all series confirmed by modified Ragone plots and ENAS factors. Also, the highest $\beta_{Li/Mg}$ for molar ratio where the lithium cations are in the minority, suggesting that the systems are highly selective in imitating actual conditions.

3.4. Selective separation of Li^+/Mg^{2+} from geothermal water

The final analysis comparing lithium and magnesium capturing by LMTO in the HCDI process evaluates their electrosorption regarding the natural, authentic geothermal sources from Western Carpathian in Poland, from Warzelnia intake. To compare the sorptive ability of HCDI, the conventional CDI with only activated carbon electrodes was selected. The measurements were carried out using the electrical modes of CV-ZVC-RCV (constant voltage- zero voltage charge- reverse constant voltage). The unique configuration consists of adsorption and double desorption steps discovered and evaluated in previous papers [60,61].

Fig. 6A and B shows particular individuals' adsorption and desorption rates for LMTO and CWZ-22 materials, respectively. Considering the LMTO material, the sorption (electrosorption) rates (blue colour) for sodium, potassium, calcium, magnesium, strontium, chlorides, hydrocarbons and boric were at the same level reached around 10% of extraction. Only for lithium and bromides, the system received 30% and 50%, respectively. A different situation is observed for CWZ-22. For standard CDI, the calcium and strontium reached 20% of sorption; for the rest, the sorption rate was 10%. The differences are also seen in desorptions steps. The green colour indicates the first desorption, while red indicates the second. This is because the first desorption was conducted without applying an electrical field. Hence, the forces from concentration differences between the new permeate solution and ion-loaded electrodes worked during this process and removed accumulated salts from the surfaces of both electrodes. Such a phenomenon was observed for each investigated system. However, only for configurations with LMTO, the desorption rate of lithium to other ions was marginally low, reached 0.25, during the first desorption and rinsed to 0.75 for the second desorption.

On the other hand, during CDI employed with CWZ-22, the release of lithium cations have the same rate during desorption one and desorption two like sodium, potassium, magnesium, chlorides, carbonates and bromide anions. Fig. 6C and D present separation factors in terms of Li/Ion. In system HCDI with LMTO material, the $\beta_{Li/Ion}$ for monovalent cations reached over 3.5. In the case of CDI employed with activated carbon, the $\beta_{Li/Ion}$ gets level below 1 for significant types of investigated elements. Considering the $\beta_{Li/Mg}$, the LMTO systems got the value at 2.5, while the activated carbon reached 1.1 during the second desorption step. According to the investigation on a binary solution, the separation factor $\beta_{Li/Mg}$ is related to the activity coefficient. The f_i got 0.68 with the molar ratio in the initial solution 1.4:1 for Li^+:Mg^{2+}. Hence, the $\beta_{Li/Mg}$ are minor during adsorption and second desorption than could be expected. However, the effect on lower $\beta_{Li/Mg}$ could be explained by a higher TDS (total dissolved salt) than in investigated binary solutions

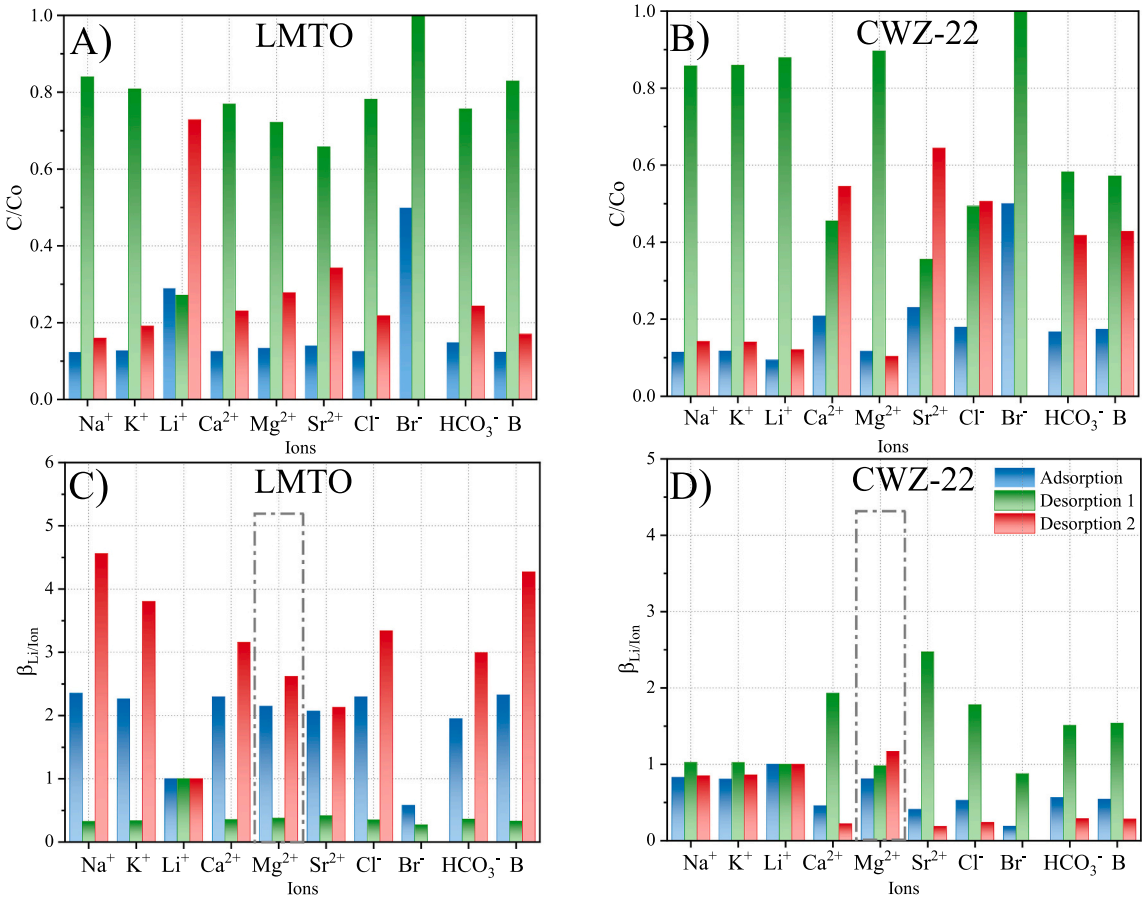

Fig. 6. The relationship of adsorption and double desorption rates for particular elements for LMTO (A) and activated carbon CWZ-22 (B) as a cathode. The separation factor is Li/Ion for LMTO (C) and activated carbon CWZ-22 (D) cathode. CV-ZVC-RCV configuration, U = 2 V, t_{ads} = 180 s, $t_{des\ 1}$ = 60 s, $t_{des\ 2}$ = 300 s. Geothermal water from the Warzelnia intake was used as the feed.

(see Table 3), which could affect the availability of capturing lithium cations.

The comparison of adsorption/desorption capacities, rates and energetical indicators with detailed concentrations of main elements are summarized in Table 5. The SAC for both materials at the charging step were similar. The main differences appeared in double desorption steps, where the SAC for D1 and D2 in system build with CWZ-22 has 60% and 40%, respectively. While during HCDI, the contribution of releasing was shifted to the first desorption with 85% removal. In the second desorption, 15% of sorbed elements were reextracted. The main distinction is visible in concentrations of particular ions. For CDI, the total extraction rate for lithium reached only 10% and 90% of this Li^+ was released at D1 flux had created a composition with a low ratio Li^+/Mg^{2+} 1:4.1. Despite HCDI, the total extraction rate reached 40.9%, and 73% of this value was released in the second desorption step.

3.5. Comparison to other processes and materials

A comparison with other materials and methods is needed to complete the lithium and magnesium separation investigation. In Table 6, the electro-membrane, membrane methods, liquid extraction and precipitation for Li^+/Mg^{2+} separations. The most mature technology applied for Li/Mg separation is general extraction. The liquid-liquid extraction applied the differences of solubility of certain salts in organic or aqueous solution for lithium removal. Due to the extractant type, the extraction process could be divided into neutral extraction and ionic liquid extraction. Among neutral extractants can be distinguished organic phosphorus salts like tributyl phosphate (TBP), which was used for Li and Mg separation from aqueous solutions [68]. The extraction contained two steps. Firstly, extraction of Li by TBP, where separation factor Li/Mg reached over 400. The second step was stripping with HCl to release extract Li from TBP. After stripping, the ratio of Mg to Li reached 1.48 [68]. The next type of extraction employed the ionic

Table 5
List of process indicators for LMTO and activated carbon as a cathode material at three stages of configuration.

Active material		SAC/SDC (mg/g)	ASAR/DSAR (mg/g·s)	ENAS/ENDS (mg/J)	Λ (arb.uni.)	C_{Li+} (mg/dm^3)	C_{Na+} (mg/dm^3)	C_{K+} (mg/dm^3)	C_{Ca2+} (mg/dm^3)	C_{Mg2+} (mg/dm^3)	C_{Sr2+} (mg/dm^3)
CWZ-22	A	777	4.32	4.76	205	1.46	981	12	28.0	5.9	5.1
(CDI)	D1	667	11.1	–	–	1.29	846	10.3	14.2	5.3	4.6
	D2	110	0.37	0.17	20.4	0.16	134	1.67	13.8	0.6	0.5
LMTO (HCDI)	A	815	4.53	2.59	120	5.28	1253	14.7	9.45	6.11	4.67
	D1	655	10.9	–	–	1.43	1053	11.9	7.27	4.41	3.07
	D2	160	0.54	1.98	238	3.85	200	2.8	2.18	1.70	1.60

Table 6
Comparison of various processes for lithium and magnesium separation.

Process	System	Li:Mg initial ratio	Conditions	Time [h]	Extraction rate of Li^+ [g/h]	$\beta_{Li/Mg}$	Ref.
Neutral extraction	tributyl phosphate	1:45	$T = 303$ K	0.3	–	403	[68]
Ionic liquid extraction	1-butyl-3-methylimidazolium hexafluorophosphate ([C4mim][PF6])	1:45	$T = 303$ K	0.3	–	125	[69]
Adsorption	Aluminium-based adsorbents	1:6	T = 303 K	2	0.0046	–	[79]
Adsorption	Manganese-based adsorbents	1.13:1	T = 303 K	72	–	599	[71]
Adsorption	Titanium-based adsorbents	1:1	T = 303 K	144	–	814	[72]
Precipitation	Organic amines	1:20	–	24	0.003	5.7	[80]
Precipitation	$MgNH_4PO_4$	1:4	pH 7–9	5	–		[81]
Nanofiltration	Membrane polyamide composite	1:5.75	Feed pressure 1.10 MPa	–	2.533	3.5	[77]
Nanofiltration	Microchannel in anion exchange membrane	1:20	Feed pressure 100 Pa		–	18.5	[73]
Nanofiltration	NF90	1:57	Feed pressure 250 kPa	–	–	2.95	[34]
Nanofiltration	PEI-TMC-DAIB	1:1	Feed pressure 8 bar	1	5.25	–	[75]
Nanofiltration	Zwitteron-carbon mitrade		Feed pressure 04 MPa	192	–	–	[76]
Dialysis	SPES-HMO	1:1	–	–	2.9	9	[82]
ED	CEM - Asahi Glass Selemion CSO	1:19	Current density 5.9A/m^2	3	1.25	20.2	[78]
ED	CEM – CIMS by ASTOM Japan	1:17	U = 5 V	2	0.025	0.08	[77]
ED	CEM - SPEEK	1:1	U = 2 V	2	0.0002	4.82	[83]
ED multi-stage	CEM - Asahi Glass Selemion CSO	1:2.8	Current 1.3A	3	0.014	~14	[84]
MCDI	CEM – CIMS by ASTOM Japan	–	U = 1 V	0.16	–	2	[42]
HCDI	LMTO material	1.4:1	U = 2 V	0.13	0.035	2.5 (geothermal)	This study
HCDI	LMTO material	1:4	U = 2 V	0.16	0.035	23	This study

liquids, typically imidazolium-based ionic liquids. By application 1-butyl-3-methylimidazolium hexafluorophosphate ([C4mim][PF6]) extractant, the separation coefficient Li/Mg reached 125 [69]. The advantages of the extraction method for separating Li and Mg can be associated with a high separation coefficient. The applied extractant, both neutral and ionic liquids, has a unique possibility to capture lithium and separate it from other ions. The disadvantages of described methods are related to a few steps of separating procedure (extraction and stripping with additional steps of filtration), high cost of compounds (ionic liquids) and relatively high amount of by-produces. Also, the regeneration steps of extractant and stripping solution could be considered a negative impact.

The following technology recommended for lithium separation from Li/Mg mixtures is an adsorption method. The critical aspect of adsorption methods for lithium recovery is the adsorption materials. The three main types of adsorbents dedicated for lithium sorption can be distinguished. Firstly, the aluminium-based adsorbents with general chemical formula $LiCl{\cdot}2Al(OH)_3{\cdot}nH_2O$. The LiAl-layered double hydroxide can selective adsorbent lithium ions based on intercalation mechanism [23], increased concentration of Li over four times that the Mg cations [70]. The second type of adsorbent recommended for lithium recovery is based on the manganese ion sieves (MnO_2) [71]. By applying this sorptive material, the separation factor Li/Mg reaches 599. The third type of adsorbent is based on titanium compounds. Typically, the layered Li_2TiO_3 or spinel $Li_4Ti_5O_{12}$ are applied for lithium sorption. TiO_2 ion-sieves were proved to have a remarkable lithium selective adsorption capacity, implying a new utilization aspect for low-dimensional titania in lithium extraction from aqueous resources, including brine or seawater [72]. The advantages of presented adsorption methods for lithium removal from aqueous solution are high separation efficiency compared with other cations, particularly with Mg^{2+}. A disadvantage of the adsorption process is a batch operation and long-time separation (72-144 h).

The other process which has found application for lithium separation is precipitation. Organic amine was employed to extract HCl formed during the CO_2 mineralization process and to realize the continuous conversion of $MgCl_2$ to precipitated $MgCO_3$, thereby removing the magnesium contained in the brine [48]. Here, the separation success is sacrificed by additional compounds that can react with Mg^{2+} and produce undissolved molecules in an aqueous solution. Then, filtration is used, and Li and Mg could be separated with high efficiency.

The following process is suitable for Li and Mg separation in nanofiltration with polyamide composite membrane. By application over 1 MPa of pressure, the extraction rate and separation achieved over 2.5 g/h and 3.5, respectively. Also, the influence of microchannels into anion exchange membrane for lithium transportation was evaluated [73]. The NF90 was applied for lithium and magnesium fractionation from natural brines, where the separation efficiency reached 85% after one cycle of nanofiltration [74]. The next type of membrane recommended for Li and Mg separation is based on a new electrolyte like diaminoethimidazole bromide, DAIB. This membrane exhibits a high lithium flux (0.97 mol/mh) with finally Mg^{2+}/Li^+ ration at 20 in permeate [75]. The Zwitterion-carbon nitrate was selected as a candidate for selective transportation magnesium cations. The Zwitterion-carbon nitrate was used as an active layer to fabricate the NF membrane. After 192 h of nanofiltration (0.4 MPa), the ratio of Mg/Li in permeate changed from 73 to 1.85 [76].

The HCDI process was compared with electrodialysis (ED). Here, the commercial membranes as a separated material, imitating acute brines solutions and a long process time in the range of 2-3 h were applied. The $\beta_{Li/Mg}$ reached from 0.08 [77] to 20.2 [78].The MCDI process is the most similar, considering the driving forces and configurations. The commercial cation exchange membranes were applied with constant voltage mode in U = 1 V. The system reached $\beta_{Li/Mg}$ at 2 points. The evaluated HCDI with LMTO as a selective material exhibited comparable $\beta_{Li/Mg}$ to ED and nanofiltration processes, reached similar values however do not require cable of hours of conducting separation. The other group of methods dedicated to Li/Mg separation is precipitation. The advantage of ED, MCDI and HCDI is a continuous operation of separation lithium and magnesium. However, the time of separation could be longer, and the separation factor of Li/Mg is lower than in the extraction of the adsorption process.

3.6. Material analysis before and after Li/Mg separation

The last stage of evaluation Li/Mg separation compares sorptive material (LMTO) before and after the HCDI process. The XRD, ^{7}Li NMR, the isotherm of N_2 accumulation to determine S_{BET} and goniometer measurements were chosen as a representative analysis.

The LMTO material was obtained according to the procedure available in [51,85]. Briefly, lithium and manganese carbonates with titanium dioxide were sintering under the air atmosphere at high temperatures to obtain spinel-type Li_x-Mn-Ti-O material. Next, the powder was treated with 0.1 M HCl to extract lithium ions and kept the spinel structure H_{x-y}-Li_y-Mn-Ti-O. Finally, the obtained material was used for cathode construction and Li/Mg separation. To understand the changes in LMTO material during Li/Mg separation, the lithium ions have been wrapped into a spinel structure during sorption. Hence, the LMTO structure came back to the initial position before extracting lithium by HCl.

In summary, the three different stages of LMTO material could be distinguished. Firstly, the material before HCl leaching with Li, material after HCl (the same as before Li/Mg separation) with underflow of Li and finally, material after Li/Mg separation with Li. The XRD patterns for evaluated materials are shown in Fig. 7A. At all stages, the LMTO material exhibited a crystal structure. The characteristic peaks at $2\theta = 19^{\circ}$ for $LiMn_2O_4$, $2\theta = 37^{\circ}$ for Mn_3O_4 and at $2\theta = 44^{\circ}$ for MnO_2. One additional peak for LMTO after Li/Mg separation appeared at $2\theta = 32^{\circ}$, and it is associated with MnO_2 [86,87]. The structure after Li/Mg separation is slightly changed with the appearance of MnO_2, and the XRD patterns are similar for LMTO before HCl treatment and after Li/Mg separation. This fact is also observed in ^{7}Li NMR in Fig. 7B. The ^{7}Li NMR spectra consist of several strongly overlapped signals, broadened due to anisotropic, quadrupole and hyperfine interactions. For LMTO after Li/Mg separation and before HCl treatment, the signal near 0 ppm could be associated with various diamagnetic lithium salts and oxides. The signals shifted to the low field present in all measured spectra, related to the lithium nuclei in structures where manganese atoms have unpaired electrons. From the values of ^{7}Li NMR isotropic chemical shifts, it is possible to check the manganese ions' valence states and discover the local crystalline structure. The signal at 1800 ppm corresponds to Li_2MnO_3, while the signal at 700–900 ppm corresponds to Li_2MnO_3 and $LiMn_2O_4$ [88–91]. For the sample before Li/Mg separation, the peaks disappeared due to HCl treatment and Li ions washed out. After Li/Mg separation (red colour), the peaks at ca. 0 ppm, 1800 ppm and 900 ppm corresponded to lithium salts and oxides appeared again.

The subsequent analysis was related to the specific surface area and polarity of the surface for LMTO at different stages. The data is presented in Table 7. The S_{BET} significantly change after HCl treatment of LMTO from ~47 to 90 m^2g^{-1}. After Li/Mg separation, the S_{BET} decreased by 20%. The shift S_{BET} to the initial value before HCl treatment cannot be possible because chloric acid exceeds the specific surface area. Also, the total surface energy (γ) was slightly changed, which can be associated with Li appearances and disappearances into the LMTO structure. Finally, the polarity of the surface (this is a ratio of the polar component to total surface energy) was detected. Here, the highest polarity was determined for LMTO after Li/Mg separation, which the accumulation of Li can also be explained into LMTO. The lowest P was detected for LMTO before HCl treatment. This effect is associated with virgin spinel and the highest Li, Mn, and Ti packages than O atoms, where O determined the polarity of the surface.

In summary, according to evaluated data of XRD, ^{7}Li NMR, S_{BET} and surface energetics, it can be concluded that the LMTO material predicts the reaction of incorporation of Li ions into its structure without deterioration of crystalline domains. The specific surface area and polarity of surfaces were slightly changed; however, it can be noticed that the LMTO, with success, has an ability of reversal reaction between Li←→H.

4. Conclusions

In the presented work, the explanation about the separation of lithium and magnesium ions from aqueous solutions, both imitated and natural brines, was studied during HCDI with LMTO as a separation material. The crucial aspects of research are summarized below:

- The HCDI employed LMTO material can conduct the lithium electrosorption reach the ideal performances in terms of sorption capacity, time, and energetical factors compared with magnesium electrosorption in the same conditions;

Table. 7
Specific surface area and surface energetics for LMTO sorbent before and after Li/Mg separation and before HCl leaching.

	Before Li/Mg separation	After Li/Mg separation	Before leaching HCl
S_{BET} (m^2g^{-1})	90.6	72.3	47.3
γ (mJ/m^2)	78.8	74.8	80.3
P (%)	36.1	38.7	31.7

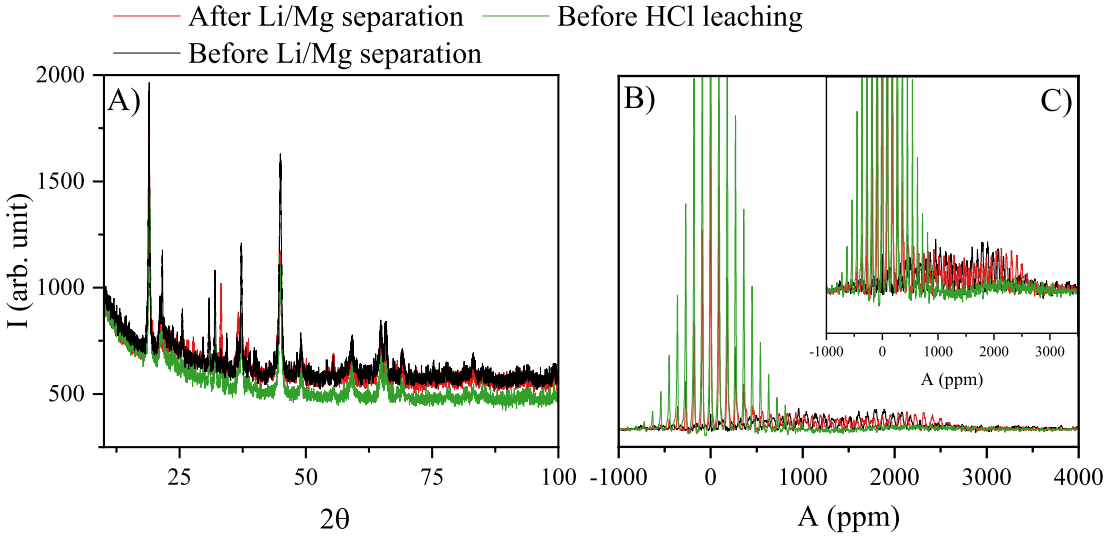

Fig. 7. X-ray patterns (A) and ^{7}Li NMR spectra (B), (C) for LMTO sorbent before and after Li/Mg separation and before HCl leaching.

- According to the Eyring-Polanyi equation, the enthalpy of activation, entropy of activation, and Gibbs energy for accumulation Li^+ and Mg^{2+} can be calculated. According to them, the lithium cation exhibits a lower value of E_a than the complex Mg^{2+}-LMTO over 15%; hence the HCDI with LMTO promoted the reaction of capturing of lithium than of accumulation magnesium ions;
- For capturing Li^+ and Mg^{2+} the requirements for self-sufficiency were met for $\Delta S‡ > 0$ and $\Delta G‡ < 0$. It meant that the LMTO material was able to sorb the Li^+ and Mg^{2+} cations;
- The separation factor $\beta_{Li/Mg}$ increase with rising the voltage value in constant voltage mode during evaluation binary solution (Li:Mg at the same molar ratio);
- The separation factor $\beta_{Li/Mg}$ increase with decreasing molar ratio of Li/Mn, reach the highest value of 23 at molar ratio Li:Mg = 0.25:1;
- The separation factor $\beta_{Li/Mg}$ strongly depends on the activity coefficient of the initial solution. With the increasing value of activity coefficient of brines, the separation factor $\beta_{Li/Mg}$ lift even when the concentration of lithium ions decreases;
- The energetical factors like ENAS felt down with decreasing separation factor $\beta_{Li/Mg}$; this phenomenon is related to the lower adsorption capacity of lithium ions;
- HCDI with LMTO material adsorbed lithium ions with $\beta_{Li/Mg}$ at 2.14 and released Li^+ with over 70% efficiency;
- LMTO material has the ability of reversal reaction between lithium and hydrogen.

CRediT authorship contribution statement

Anna Siekierka designed and performed experiments, analysed, calculated and discussed all of data related with enclosed manuscript. Anna Siekierka wrote and revise manuscript. AS provide the financial support.

Declaration of competing interest

AS declared that she has not known competing for financial interests or personal relationships that could have influenced the work reported in this paper.

Acknowledgements

AS would like to thank prof. Barbara Tomaszewska for geothermal water delivery and carry out analyses of element concentrations.

AS would like to thank the Department of Process Engineering and Technology of Polymeric and Carbon Materials, Wroclaw University of Science and Technology, for financial support from the ministerial subsidy.

AS is supported by the Polish Ministry of Education and Science under the programme for outstanding young scientists.

AS is supported by Foundation for Polish Science (START) under project number 075.2021.

References

[1] Y. Sun, Q. Wang, Y. Wang, R. Yun, X. Xiang, Recent advances in magnesium/lithium separation and lithium extraction technologies from salt lake brine, Sep. Purif. Technol. 256 (2021), 117807, https://doi.org/10.1016/j.seppur.2020.117807.

[2] W. Xu, L. He, Z. Zhao, Lithium extraction from high Mg/Li brine via electrochemical intercalation/de-intercalation system using LiMn2O4 materials, Desalination 503 (2021), 114935, https://doi.org/10.1016/j.desal.2021.114935.

[3] T. Hoshino, Development of technology for recovering lithium from seawater by electrodialysis using ionic liquid membrane, Fusion Eng. Des. 88 (2013) 2956–2959, https://doi.org/10.1016/j.fusengdes.2013.06.009.

[4] F. Meng, J. McNeice, S.S. Zadeh, A. Ghahreman, Review of lithium production and recovery from minerals, brines, and lithium-ion batteries, Miner. Process. Extr. Metall. Rev. (2019) 1–19, https://doi.org/10.1080/08827508.2019.1668387.

[5] S.H. Mohr, G.M. Mudd, D. Giurco, Lithium resources and production: critical assessment and global projections, Minerals 2 (2012) 65–84, https://doi.org/10.3390/min2010065.

[6] A. Siekierka, Lithium iron manganese oxide as an adsorbent for capturing lithium ions in hybrid capacitive deionization with different electrical modes, Sep. Purif. Technol. 236 (2020), https://doi.org/10.1016/j.seppur.2019.116234.

[7] Y. Zhao, M. Wu, P. Shen, C. Uytterhoeven, N. Mamrol, J. Shen, C. Gao, B. Van der Bruggen, Composite anti-scaling membrane made of interpenetrating networks of nanofibers for selective separation of lithium, J. Memb. Sci. 618 (2021), 118668, https://doi.org/10.1016/j.memsci.2020.118668.

[8] G. Rayner-Canham, Isodiagonality in the periodic table, Found. Chem. 13 (2011) 121–129, https://doi.org/10.1007/s10698-011-9108-y.

[9] G. Kuang, Y. Liu, H. Li, S. Xing, F. Li, H. Guo, Extraction of lithium from β-spodumene using sodium sulfate solution, Hydrometallurgy. 177 (2018) 49–56, https://doi.org/10.1016/j.hydromet.2018.02.015.

[10] Q. Li, H. Liu, B. He, W. Shi, Y. Ji, Z. Cui, F. Yan, Y. Mohammad, J. Li, Ultrahigh-efficient separation of Mg2+/Li+ using an in-situ reconstructed positively charged nanofiltration membrane under an electric field, J. Memb. Sci. 641 (2022), 119880, https://doi.org/10.1016/J.MEMSCI.2021.119880.

[11] Y. Marcus, Thermodynamics of solvation of ions. Part 5. —Gibbs free energy of hydration at 298.15 K, J. Chem. Soc. Faraday Trans. 87 (1991) 2995–2999, https://doi.org/10.1039/FT9918702995.

[12] O. Reckeweg, F. Lissner, B. Blaschkowski, P. Gross, H.A. Höppe, T. Schleid, Two light-metal dihydrogenisocyanurate hydrates linked by diagonal relationship: syntheses, crystal structures, and vibrational spectra of Li[H2N3C3O3]·1.75 H2O and Mg[H2N3C3O3]2·8 H2O, Z. Anorg. Allg.Chem. 646 (2020) 1252–1259, https://doi.org/10.1002/zaac.202000015.

[13] D. Kalden, A. Oberheide, C. Loh, H. Görls, S. Krieck, M. Westerhausen, Surprisingly different reaction behavior of alkali and alkaline earth metal Bis(trimethylsilyl) amides toward bulky N-(2-Pyridylethyl)-N′-(2,6-diisopropylphenyl)pivalamidine, Chem. A Eur. J. 22 (2016) 10944–10959, https://doi.org/10.1002/chem.201602074.

[14] Y. Zhao, H. Wang, Y. Li, M. Wang, X. Xiang, An integrated membrane process for preparation of lithium hydroxide from high Mg/Li ratio salt lake brine, Desalination 493 (2020), 114620, https://doi.org/10.1016/j.desal.2020.114620.

[15] Y.P. Tang, L. Luo, Z. Thong, T.S. Chung, Recent advances in membrane materials and technologies for boron removal, J. Memb. Sci. 541 (2017) 434–446, https://doi.org/10.1016/j.memsci.2017.07.015.

[16] H. Su, Z. Li, J. Zhang, W. Liu, Z. Zhu, L. Wang, T. Qi, Combining selective extraction and easy stripping of lithium using a ternary synergistic solvent extraction system through regulation of Fe3+ coordination, ACS Sustain. Chem. Eng. 8 (2020) 1971–1979, https://doi.org/10.1021/acssuschemeng.9b06432.

[17] D. Gao, X. Yu, Y. Guo, S. Wang, M. Liu, T. Deng, Y. Chen, N. Belzile, Extraction of lithium from salt lake brine with triisobutyl phosphate in ionic liquid and kerosene, Chem. Res. Chin. Univ. 31 (2015) 621–626, https://doi.org/10.1007/s40242-015-4376-z.

[18] G.T. Wei, Z. Yang, C.J. Chen, Room temperature ionic liquid as a novel medium for liquid/liquid extraction of metal ions, Anal. Chim. Acta 488 (2003) 183–192, https://doi.org/10.1016/S0003-2670(03)00660-3.

[19] R. Bai, J. Wang, D. Wang, Y. Zhang, J. Cui, Selective separation of lithium from the high magnesium brine by the extraction system containing phosphate-based ionic liquids, Sep. Purif. Technol. 274 (2021), 119051, https://doi.org/10.1016/J.SEPPUR.2021.119051.

[20] Z. Zhou, W. Qin, W. Fei, Extraction equilibria of lithium with tributyl phosphate in three diluents, J. Chem. Eng. Data 56 (2011) 3518–3522, https://doi.org/10.1021/je200246x.

[21] Z. Zhou, W. Qin, W. Fei, Y. Li, A study on stoichiometry of complexes of tributyl phosphate and methyl isobutyl ketone with lithium in the presence of FeCl 3, Chin. J. Chem. Eng. 20 (2012) 36–39, https://doi.org/10.1016/S1004-9541(12)60360-7.

[22] W. Chen, X. Li, L. Chen, G. Zhou, Q. Lu, Y. Huang, Y. Chao, W. Zhu, Tailoring hydrophobic deep eutectic solvent for selective lithium recovery from the mother liquor of Li2CO3, Chem. Eng. J. 420 (2021), 127648, https://doi.org/10.1016/J.CEJ.2020.127648.

[23] V.P. Isupov, N.P. Kotsupalo, A.P. Nemudry, L.T. Menzeres, Aluminium hydroxide as selective sorbent of lithium salts from brines and technical solutions, Stud. Surf. Sci. Catal. 120 (A) (1999) 621–652, https://doi.org/10.1016/s0167-2991(99)80567-9.

[24] K.H. Goh, T.T. Lim, Z. Dong, Application of layered double hydroxides for removal of oxyanions: a review, Water Res. 42 (2008) 1343–1368, https://doi.org/10.1016/j.watres.2007.10.043.

[25] A.V. Besserguenev, A.M. Fogg, R.J. Francis, S.J. Price, D. O'Hare, V.P. Isupov, B. P. Tolochko, Synthesis and structure of the gibbsite intercalation compounds [LiAl2(OH)6]X X = Cl, Br, NO3 and [LiAl2(OH)6]Cl·H2O using synchrotron X-ray and neutron powder diffraction, Chem. Mater. 9 (1997) 241–247, https://doi.org/10.1021/cm960316z.

[26] C. Zhao, R. Ge, Y. Zhen, Y. Wang, Z. Li, Y. Shi, X. Chen, A hybrid process of coprecipitation-induced crystallization-capacitive deionization-ion exchange process for heavy metals removal from hypersaline ternary precursor wastewater, Chem. Eng. J. 378 (2019), 122136, https://doi.org/10.1016/j.cej.2019.122136.

[27] W. Xiao, C. Xin, S. Li, J. Jie, Y. Gu, J. Zheng, F. Pan, Insight into fast li diffusion in li-excess spinel lithium manganese oxide, J. Mater. Chem. A 6 (2018) 9893–9898, https://doi.org/10.1039/c8ta01428k.

[28] Y. Wang, J. Xu, X. Xu, D. Yang, X. Zheng, J. Pan, T. Zhang, F. Qiu, C. Li, Mesoporous hollow silicon spheres modified with manganese ion sieve:

preparation and its application for adsorption of lithium and rubidium ions, Appl. Organomet. Chem. 32 (2018), e4182, https://doi.org/10.1002/aoc.4182.
[29] R. Chitrakar, Y. Makita, K. Ooi, A. Sonoda, Lithium recovery from salt lake brine by H2TiO3, Dalt. Trans. 43 (2014) 8933–8939, https://doi.org/10.1039/c4dt00467a.
[30] Q.H. Zhang, S.P. Li, S.Y. Sun, X.S. Yin, J.G. Yu, Lithium selective adsorption on low-dimensional titania nanoribbons, Chem. Eng. Sci. 65 (2010) 165–168, https://doi.org/10.1016/j.ces.2009.06.001.
[31] X. Guo, S. Hu, C. Wang, H. Duan, X. Xiang, Highly efficient separation of magnesium and lithium and high-valued utilization of magnesium from salt Lake brine by a reaction-coupled separation technology, Ind. Eng. Chem. Res. 57 (2018) 6618–6626, https://doi.org/10.1021/acs.iecr.8b01147.
[32] R. Marthi, Y.R. Smith, Application and limitations of a H2TiO3 – diatomaceous earth composite synthesized from titania slag as a selective lithium adsorbent, Sep. Purif. Technol. 254 (2021), 117580, https://doi.org/10.1016/J.SEPPUR.2020.117580.
[33] Q. Bi, Z. Zhang, C. Zhao, Z. Tao, Study on the recovery of lithium from high Mg2+/Li+ ratio brine by nanofiltration, Water Sci. Technol. 70 (2014) 1690–1694, https://doi.org/10.2166/wst.2014.426.
[34] A. Somrani, A.H. Hamzaoui, M. Pontie, Study on lithium separation from salt lake brines by nanofiltration (NF) and low pressure reverse osmosis (LPRO), Desalination 317 (2013) 184–192, https://doi.org/10.1016/j.desal.2013.03.009.
[35] Q. Bi, S. Xu, Separation of magnesium and lithium from brine with high Mg2+/Li+ ratio by a two-stage nanofiltration process, 2018, https://doi.org/10.5004/dwt.2018.23062.
[36] L. Gong, W. Ouyang, Z. Li, J. Han, Direct numerical simulation of continuous lithium extraction from high Mg2+/Li+ ratio brines using microfluidic channels with ion concentration polarization, J. Memb. Sci. 556 (2018) 34–41, https://doi.org/10.1016/j.memsci.2018.03.078.
[37] D. Lu, T. Ma, S. Lin, Z. Zhou, G. Li, Q. An, Z. Yao, Q. Sun, Z. Sun, L. Zhang, Constructing a selective blocked-nanolayer on nanofiltration membrane via surface-charge inversion for promoting Li+ permselectivity over Mg2+, J. Membr. Sci. 635 (2021), 119504 https://doi.org/10.1016/J.MEMSCI.2021.119504.
[38] X.Y. Nie, S.Y. Sun, Z. Sun, X. Song, J.G. Yu, Ion-fractionation of lithium ions from magnesium ions by electrodialysis using monovalent selective ion-exchange membranes, Desalination 403 (2017) 128–135, https://doi.org/10.1016/j.desal.2016.05.010.
[39] T. Xu, Ion exchange membranes: state of their development and perspective, J. Membr. Sci. 263 (2005) 1–29, https://doi.org/10.1016/j.memsci.2005.05.002.
[40] X. Liu, X. Chen, L. He, Z. Zhao, Study on extraction of lithium from salt lake brine by membrane electrolysis, Desalination 376 (2015) 35–40, https://doi.org/10.1016/j.desal.2015.08.013.
[41] S. Bunani, N. Kabay, S. Bunani, M. Arda, K. Yoshizuka, S. Nishihama, S. Bunani, Effect of process conditions on recovery of lithium and boron from water using bipolar membrane electrodialysis (BMED), Desalination 416 (2017) 10–15, https://doi.org/10.1016/j.desal.2017.04.017.
[42] W. Shi, X. Liu, C. Ye, X. Cao, C. Gao, J. Shen, Efficient lithium extraction by membrane capacitive deionization incorporated with monovalent selective cation exchange membrane, Sep. Purif. Technol. 210 (2019) 885–890, https://doi.org/10.1016/j.seppur.2018.09.006.
[43] T. Ryu, D.H. Lee, J.C. Ryu, J. Shin, K.S. Chung, Y.H. Kim, Lithium recovery system using electrostatic field assistance, Hydrometallurgy 151 (2015) 78–83, https://doi.org/10.1016/j.hydromet.2014.11.005.
[44] X. Xu, Y. Zhou, Z. Feng, N.U. Kahn, Z.U. Haq Khan, Y. Tang, Y. Sun, P. Wan, Y. Chen, M. Fan, A self-supported λ-MnO2 film electrode used for electrochemical lithium recovery from brines, Chempluschem. 83 (2018) 521–528, https://doi.org/10.1002/cplu.201800185.
[45] S. Kim, J. Lee, S. Kim, S. Kim, J. Yoon, Electrochemical lithium recovery with a LiMn2O4–Zinc battery system using zinc as a negative electrode, Energy Technol. 6 (2018) 340–344, https://doi.org/10.1002/ente.201700488.
[46] M. Lee, W. Jung, H.J. Kwon, G. Lim, Continuous ion separation via electrokinetic-driven ion migration path differentiation: practical application to lithium extraction from brines, J. Mater. Chem. A (2022), https://doi.org/10.1039/D1TA08162D.
[47] Z. Zhao, X. Si, X. Liu, L. He, X. Liang, Li extraction from high Mg/Li ratio brine with LiFePO4/FePO4 as electrode materials, Hydrometallurgy 133 (2013) 75–83, https://doi.org/10.1016/J.HYDROMET.2012.11.013.
[48] P. Chen, S. Tang, H. Yue, C. Liu, C. Li, B. Liang, Lithium enrichment of high Mg/Li ratio brine by precipitation of magnesium via combined CO 2 mineralization and solvent extraction, Ind. Eng. Chem. Res. 56 (2017) 5668–5678, https://doi.org/10.1021/acs.iecr.6b04892.
[49] P. Meshram, B.D. Pandey, T.R. Mankhand, Extraction of lithium from primary and secondary sources by pre-treatment, leaching and separation: a comprehensive review, Hydrometallurgy. 150 (2014) 192–208, https://doi.org/10.1016/J.HYDROMET.2014.10.012.
[50] J. Sterba, A. Krzemień, G.Fidalgo Valverde, I.Diego Álvarez, C. Castañón Fernández, Energy-sustainable industrialized growth in the Czech Republic: the Cínovec lithium mining project, Resour. Policy 68 (2020), 101707, https://doi.org/10.1016/j.resourpol.2020.101707.
[51] A. Siekierka, J. Kujawa, W. Kujawski, M. Bryjak, Lithium dedicated adsorbent for the preparation of electrodes useful in the ion pumping method, Sep. Purif. Technol. 194 (2018) 231–238, https://doi.org/10.1016/j.seppur.2017.11.045.
[52] H. Vikström, S. Davidsson, M. Höök, Lithium availability and future production outlooks, Appl. Energy 110 (2013) 252–266, https://doi.org/10.1016/J.APENERGY.2013.04.005.
[53] K. Singh, H.J.M. Bouwmeester, L.C.P.M. De Smet, M.Z. Bazant, P.M. Biesheuvel, Theory of water desalination with intercalation materials, Phys. Rev. Appl. 9 (2018), https://doi.org/10.1103/PhysRevApplied.9.064036.
[54] W. Tang, J. Liang, D. He, J. Gong, L. Tang, Z. Liu, D. Wang, G. Zeng, Various cell architectures of capacitive deionization: recent advances and future trends, Water Res. 150 (2019) 225–251, https://doi.org/10.1016/J.WATRES.2018.11.064.
[55] M.E. Suss, S. Porada, X. Sun, P.M. Biesheuvel, J. Yoon, V. Presser, Water desalination via capacitive deionization: what is it and what can we expect from it? Energy Environ. Sci. 8 (2015) 2296–2319, https://doi.org/10.1039/c5ee00519a.
[56] J. Lee, S. Kim, C. Kim, J. Yoon, Hybrid capacitive deionization to enhance the desalination performance of capacitive techniques, Energy Environ. Sci. 7 (2014) 3683–3689, https://doi.org/10.1039/C4EE02378A.
[57] A. Siekierka, E. Kmiecik, B. Tomaszewska, K. Wator, M. Bryjak, The evaluation of the effectiveness of lithium separation by hybrid capacitive deionization from geothermal water with the uncertainty measurement application, Desalin. Water Treat. 128 (2018) 259–264, https://doi.org/10.5004/dwt.2018.22870.
[58] A. Siekierka, M. Bryjak, J. Wolska, The use of activated carbon modified with polypyrrole as a supporting electrode for lithium ions adsorption in capacitive deionization, Desalin. Water Treat. 64 (2017) 251–254, https://doi.org/10.5004/dwt.2017.11387.
[59] A. Siekierka, Preparation of electrodes for hybrid capacitive deionization and its influence on the adsorption behaviour, Sep. Sci. Technol. (2019) 1–12, https://doi.org/10.1080/01496395.2019.1609032.
[60] A. Siekierka, B. Tomaszewska, M. Bryjak, Lithium capturing from geothermal water by hybrid capacitive deionization, Desalination 436 (2018) 8–14, https://doi.org/10.1016/j.desal.2018.02.003.
[61] A. Siekierka, Lithium iron manganese oxide as an adsorbent for capturing lithium ions in hybrid capacitive deionization with different electrical modes, Sep. Purif. Technol. (2019), https://doi.org/10.1016/j.seppur.2019.116234.
[62] A. Siekierka, M. Bryjak, Hybrid capacitive deionization with anion-exchange membranes for lithium extraction, E3S Web Conf. 22 (2017) 00157, https://doi.org/10.1051/e3sconf/20172200157.
[63] A. Siekierka, J. Wolska, W. Kujawski, M. Bryjak, Modification of poly(vinyl chloride) films by aliphatic amines to prepare anion-exchange membranes for cr (VI) removal, Sep. Sci. Technol. 53 (2018) 1191–1197, https://doi.org/10.1080/01496395.2017.1358746.
[64] A. Siekierka, J. Wolska, M. Bryjak, W. Kujawski, Anion exchange membranes in lithium extraction by means of capacitive deionization system, Desalin. Water Treat. 75 (2017) 331–341, https://doi.org/10.5004/dwt.2017.20431.
[65] J. Sreńscek-Nazzal, U. Narkiewicz, A.W. Morawski, R.J. Wróbel, B. Michalkiewicz, The increase of the micoporosity and CO2 adsorption capacity of the commercial activated carbon CWZ-22 by KOH treatment, Microporous Mesoporous Mater. (2016), https://doi.org/10.5772/63672.
[66] T. Kim, J. Yoon, CDI ragone plot as a functional tool to evaluate desalination performance in capacitive deionization, RSC Adv. 5 (2015) 1456–1461, https://doi.org/10.1039/C4RA11257A.
[67] L. Agartan, B. Akuzum, E. Agar, E.C. Kumbur, Impact of flow configuration on electrosorption performance and energy consumption of CDI systems, J. Water Supply Res Technol. 69 (2020) 134–144, https://doi.org/10.2166/AQUA.2020.012.
[68] C. Shi, Y. Jing, Y. Jia, Solvent extraction of lithium ions by tri-n-butyl phosphate using a room temperature ionic liquid, J. Mol. Liq. 215 (2016) 640–646, https://doi.org/10.1016/J.MOLLIQ.2016.01.025.
[69] C. Shi, D. Duan, Y. Jia, Y. Jing, A highly efficient solvent system containing ionic liquid in tributyl phosphate for lithium ion extraction, J. Mol. Liq. 200 (2014) 191–195, https://doi.org/10.1016/J.MOLLIQ.2014.10.004.
[70] H. Jiang, Y. Yang, S. Sun, J. Yu, Adsorption of lithium ions on lithium-aluminum hydroxides: equilibrium and kinetics, Can. J. Chem. Eng. 98 (2020) 544–555, https://doi.org/10.1002/CJCE.23640.
[71] Q.H. Zhang, S.P. Li, S.Y. Sun, X.S. Yin, J.G. Yu, Lithium selective adsorption on 1-D MnO2 nanostructure ion-sieve, Adv. Powder Technol. 20 (2009) 432–437, https://doi.org/10.1016/J.APT.2009.02.008.
[72] Q.H. Zhang, S.P. Li, S.Y. Sun, X.S. Yin, J.G. Yu, Lithium selective adsorption on low-dimensional titania nanoribbons, Chem. Eng. Sci. 65 (2010) 165–168, https://doi.org/10.1016/J.CES.2009.06.001.
[73] L. Gong, W. Ouyang, Z. Li, J. Han, Direct numerical simulation of continuous lithium extraction from high Mg2+/Li+ ratio brines using microfluidic channels with ion concentration polarization, J. Membr. Sci. 556 (2018) 34–41, https://doi.org/10.1016/J.MEMSCI.2018.03.078.
[74] A. Somrani, A.H. Hamzaoui, M. Pontie, Study on lithium separation from salt lake brines by nanofiltration (NF) and low pressure reverse osmosis (LPRO), Desalination 317 (2013) 184–192, https://doi.org/10.1016/J.DESAL.2013.03.009.
[75] H. Peng, Q. Zhao, H. Peng, Q. Zhao, A Nano-heterogeneous membrane for efficient separation of lithium from high Magnesium/Lithium ratio brine, Adv. Funct. Mater. 31 (2021) 2009430, https://doi.org/10.1002/ADFM.202009430.
[76] Q. Bi, C. Zhang, J. Liu, X. Liu, S. Xu, Positively charged zwitterion-carbon nitride functionalized nanofiltration membranes with excellent separation performance of Mg2+/Li+ and good antifouling properties, Sep. Purif. Technol. 257 (2021), 117959, https://doi.org/10.1016/J.SEPPUR.2020.117959.
[77] Z.Yong Ji, Q.Bai Chen, J.Sheng Yuan, J. Liu, Y.Ying Zhao, W.Xian Feng, Preliminary study on recovering lithium from high Mg2+/Li+ ratio brines by electrodialysis, Sep. Purif. Technol. 172 (2017) 168–177, https://doi.org/10.1016/J.SEPPUR.2016.08.006.
[78] X.Y. Nie, S.Y. Sun, Z. Sun, X. Song, J.G. Yu, Ion-fractionation of lithium ions from magnesium ions by electrodialysis using monovalent selective ion-exchange

membranes, Desalination 403 (2017) 128–135, https://doi.org/10.1016/J.DESAL.2016.05.010.
[79] J. Zhong, S. Lin, J. Yu, Effects of excessive lithium deintercalation on Li+ adsorption performance and structural stability of lithium/aluminum layered double hydroxides, J. Colloid Interface Sci. 572 (2020) 107–113, https://doi.org/10.1016/J.JCIS.2020.03.081.
[80] P. Chen, S. Tang, H. Yue, C. Liu, C. Li, B. Liang, Lithium enrichment of high Mg/Li ratio brine by precipitation of magnesium via combined CO2 mineralization and solvent extraction, Ind. Eng. Chem. Res. 56 (2017) 5668–5678, https://doi.org/10.1021/ACS.IECR.6B04892/SUPPL_FILE/IE6B04892_SI_001.PDF.
[81] L. He, W. Xu, Y. Song, X. Liu, Z. Zhao, Selective removal of magnesium from a lithium-concentrated anolyte by magnesium ammonium phosphate precipitation, Sep. Purif. Technol. 187 (2017) 214–220, https://doi.org/10.1016/J.SEPPUR.2017.04.028.
[82] H.M. Saif, R.M. Huertas, S. Pawlowski, J.G. Crespo, S. Velizarov, Development of highly selective composite polymeric membranes for Li+/Mg2+ separation, J. Membr. Sci. 620 (2021), 118891, https://doi.org/10.1016/J.MEMSCI.2020.118891.
[83] P.P. Sharma, V. Yadav, A. Rajput, H. Gupta, H. Saravaia, V. Kulshrestha, Sulfonated poly (ether ether ketone) composite cation exchange membrane for selective recovery of lithium by electrodialysis, Desalination 496 (2020), 114755, https://doi.org/10.1016/J.DESAL.2020.114755.
[84] J. Ying, M. Luo, Y. Jin, J. Yu, Selective separation of lithium from high Mg/Li ratio brine using single-stage and multi-stage selective electrodialysis processes, Desalination 492 (2020), 114621, https://doi.org/10.1016/J.DESAL.2020.114621.
[85] A. Siekierka, M. Bryjak, Selective sorbents for recovery of lithium ions by hybrid capacitive deionization, Desalination 520 (2021), 115324, https://doi.org/10.1016/J.DESAL.2021.115324.
[86] L. Feng, Z. Xuan, H. Zhao, Y. Bai, J. Guo, C.Wei Su, X. Chen, MnO2 prepared by hydrothermal method and electrochemical performance as anode for lithium-ion battery, Nanoscale Res. Lett. 9 (2014) 1–8, https://doi.org/10.1186/1556-276X-9-290/TABLES/1.
[87] X. Wan, S. Yang, Z. Cai, Q. He, Y. Ye, Y. Xia, G. Li, J. Liu, Facile synthesis of MnO2 nanoflowers/N-doped reduced graphene oxide composite and its application for simultaneous determination of dopamine and uric acid, Nanomaterials 9 (2019) 847, https://doi.org/10.3390/NANO9060847.
[88] M.C. Tucker, J.A. Reimer, E.J. Cairns, A [sup 7]Li nuclear magnetic resonance study of metal-substituted lithium manganese oxide spinels, J. Electrochem. Soc. 148 (2001) A951, https://doi.org/10.1149/1.1383775.
[89] E.M. Stephens, C.M. Grisham, Lithium-7 nuclear magnetic resonance, water proton nuclear magnetic resonance, and gadolinium electron paramagnetic resonance studies of the sarcoplasmic reticulum calcium ion transport adenosine triphosphatase, Biochemistry 18 (1979) 4876–4885, https://doi.org/10.1021/bi00589a016.
[90] Y.J. Lee, F. Wang, C.P. Grey, 6Li and 7Li MAS NMR studies of lithium manganate cathode materials, J. Am. Chem. Soc. 120 (1998) 12601–12613, https://doi.org/10.1021/ja9817794.
[91] E. Bekaert, F. Robert, P.E. Lippens, M. Ménétrier, 7Li NMR knight shifts in li-sn compounds: MAS NMR measurements and correlation with DFT calculations, J. Phys. Chem. C 114 (2010) 6749–6754, https://doi.org/10.1021/jp100365u.